

1 **Wintertime organic and inorganic aerosols in Lanzhou, China:**
2 **Sources, processes and comparison with the results during**
3 **summer**

4

5 **J. Xu¹, J. Shi², Q. Zhang³, X. Ge⁴, F. Canonaco⁵, A. S. H. Prévôt^{5,6}, M. Vonwiller⁷, S.**
6 **Szidat⁷, J. Ge², J. Ma⁸, Y. An¹, S. Kang¹, D. Qin¹**

7 ¹State Key Laboratory of Cryospheric Sciences, Cold and Arid Regions Environmental
8 and Engineering Research Institute, CAS, Lanzhou 730000, China

9 ²Key Laboratory for Semi-Arid Climate Change of the Ministry of Education, College of
10 Atmospheric Sciences, Lanzhou University, Lanzhou 730000, China

11 ³Department of Environmental Toxicology, University of California, Davis, CA 95616,
12 USA

13 ⁴Jiangsu Key Laboratory of Atmospheric Environment Monitoring and Pollution Control
14 (AEMPC), School of Environmental Science and Engineering, Nanjing University of
15 Information Science & Technology, Nanjing 210044, China

16 ⁵Laboratory of Atmospheric Chemistry, Paul Scherrer Institute (PSI), Villigen 5232,
17 Switzerland

18 ⁶State Key Laboratory of Loess and Quaternary Geology and Key Laboratory of Aerosol
19 Chemistry and Physics, Institute of Earth Environment, Chinese Academy of Sciences,
20 710075 Xi'an, China

21 ⁷Department of Chemistry and Biochemistry & Oeschger Centre for Climate Change
22 Research, University of Bern, Berne, 3012, Switzerland

23 ⁸College of Earth Environmental Science, Lanzhou University, Lanzhou 730000, China

24

25 Correspondence to: J. Xu (jzxu@lzb.ac.cn)

26

27 **Abstract**

28 Lanzhou, which is located in a steep Alpine valley in western China, is one of the most
29 polluted cities in China during the wintertime. In this study, an Aerodyne high resolution
30 time-of-flight aerosol mass spectrometer (HR-ToF-AMS), a seven-wavelength
31 aethalometer, and a scanning mobility particle sizer (SMPS) were deployed during
32 January 10 to February 4, 2014 to study the mass concentrations, chemical processes, and
33 sources of sub-micrometer particulate matter (PM₁). The average PM₁ concentration
34 during this study was 57.3 µg m⁻³ (ranging from 2.1 to 229.7 µg m⁻³ for hourly averages)
35 with organic aerosol (OA) accounting for 51.2%, followed by nitrate (16.5%), sulphate
36 (12.5%), ammonium (10.3%), black carbon (BC, 6.4%), and chloride (3.0%). The mass
37 concentration of PM₁ during winter was more than twice the average value observed at
38 the same site in summer 2012 (24.5 µg m⁻³), but the mass fraction of OA was similar in
39 the two seasons. Nitrate contributed a significantly higher fraction to the PM₁ mass in
40 winter compared to summer, largely due to more favoured partitioning to the particle
41 phase at low air temperature. The mass fractions of both OA and nitrate increased by ~5%
42 (49% to 53% for OA and 13% to 18% for nitrate) with the increase of the total PM₁ mass
43 loading, while the average sulphate fraction decreased by 6% (17% to 11%), indicating
44 the importance of OA and nitrate for the heavy air pollution events in Lanzhou. The size
45 distributions of OA, nitrate, sulphate, ammonium, and chloride all peaked at ~500 nm
46 with OA being slightly broader, suggesting that aerosol particles were internally mixed
47 during winter, likely due to frequently calm and stagnant air conditions during wintertime
48 in Lanzhou (average wind speed: 0.82 m s⁻¹).

49

50 The average mass spectrum of OA showed a medium oxidation degree (average O/C
51 ratio of 0.28), which was lower than that during summer 2012 (O/C = 0.33). This is
52 consistent with weaker photochemical processing during winter. Positive matrix
53 factorization (PMF) with the multi-linear engine (ME-2) solver identified six OA sources,
54 i.e., a hydrocarbon-like OA (HOA), a biomass burning OA (BBOA), a cooking-emitted

55 OA (COA), a coal combustion OA (CCOA), and two oxygenated OA (OOA) factors.
56 One of the OOAs was less-oxidized (LO-OOA) and the other one of more-oxidized (MO-
57 OOA). LO-OOA was the most abundant OA component (24% of OA mass), followed by
58 COA (20%), MO-OOA (19%), CCOA (18%), BBOA (11%), and HOA (9%). The mass
59 fraction of primary OA (= HOA + BBOA + COA + CCOA) increased during high PM
60 pollution periods, indicating that local primary emissions were a main reason for the
61 formation of air pollution events in Lanzhou during winter. Radiocarbon (^{14}C)
62 measurement was conducted on four $\text{PM}_{2.5}$ filter samples from this study, which allowed
63 for a quantitative source apportionment of organic carbon (OC). The non-fossil sources
64 on average accounted for $55 \pm 3\%$ of OC which could be mainly from biomass burning
65 and cooking activities, suggesting the importance of non-fossil sources for the PM
66 pollution in Lanzhou. Combining with the PMF results, we also found that a large
67 fraction (57%) of the secondary OC was from non-fossil OC.

68

69 **1 Introduction**

70 Frequent haze pollution events in urban areas in China have been a widespread concern
71 in recent years due to its high adverse health effects, visibility degradation and climate
72 effects (Chan and Yao, 2008). The Chinese Central Government had put in extensive
73 efforts to find urgent and suitable control strategies to reduce further deterioration of air
74 quality. Strategies such as promoting energy conservation and emission reduction
75 measures and new air quality standards ($\text{PM}_{2.5}$ currently vs. PM_{10} in the past) have been
76 implemented in the last three years ([http://www.gov.cn/zwggk/2013-
77 09/12/content_2486773.htm](http://www.gov.cn/zwggk/2013-09/12/content_2486773.htm)). Many local governments have also launched measures such
78 as shutting down some highly polluting factories and restricting the use of private
79 vehicles to reduce air pollution in their cities. However, air pollution in China is still far
80 from being controlled due to its complex sources and limited knowledge on the multiple
81 pathways leading to secondary aerosol formation and dynamic variation of aerosol mass
82 loading.

83

84 Lanzhou, the capital of Gansu province, is located at the northwest of China and has
85 experienced air pollution issues since the 1960s due to emissions from the petrochemical
86 industry and its valley terrain which tended to form stagnant meteorological conditions
87 (Tang et al., 1985; Zhang et al., 2000). Air pollution is still serious and has become more
88 variable in recent years (since 2000) because of fast urbanization and increased energy
89 consumption. The severity of air pollution often reaches maximum intensity during
90 winter due to coal combustion for domestic heating and cooking, similar to the situations
91 in most cities of northern China (Wang et al., 2014). Despite the serious air pollution
92 during winter in Lanzhou, aerosol chemistry, sources, and formation and transformation
93 processes were poorly documented in the literature, which limit the development and
94 implementation of efficient control strategies.

95

96 The chemical and physical properties of atmospheric aerosol particles during winter,
97 especially during haze episode, have been recently investigated in metropolitan cities in
98 Eastern China (Sun et al., 2006; Zhao et al., 2013; Huang et al., 2014; Sun et al., 2014).
99 For example, the mean aerosol optical depth at 500 nm were up to ~0.7 during the month-
100 long heavy haze pollution episode during January 2013 in Beijing (Bi et al., 2014); The
101 airborne microbes were found in particulate matter (PM) during hazy period which may
102 potentially include respiratory microbial allergens and pathogens (Cao et al., 2014).
103 Collection and analysis of filter samples have enabled quantification of the chemical
104 composition of PM using a suite of off-line instruments (such as ion chromatography,
105 organic and element carbon analyzer, inductively coupled plasma-mass spectrometry and
106 so on) in the laboratory (He et al., 2001; Zheng et al., 2005; Sun et al., 2006; Sun et al.,
107 2011a; Zhang et al., 2013; Zhao et al., 2013), but often incapable of capturing details of
108 the atmospheric evolution processes during the typical lifecycle of aerosol.

109

110 Previous studies on source apportionment of aerosol particle identified dust, traffic,
111 industry, cooking-related activities, and secondary formation as important contributors,
112 although the contributions of individual sources may change drastically with location,

113 season, and different apportionment algorithms (Zheng et al., 2005; Yu et al., 2013;
114 Huang et al., 2014). For example, Zheng et al. (2005) used chemical mass balance
115 (CMB) receptor model to quantitatively apportion the sources that contribute to fine PM
116 concentration in Beijing and found coal combustion contributed 16% of fine PM mass in
117 January. By contrast, principal component analysis of the same dataset estimated almost
118 twice amount of aerosols from coal combustion (Song et al., 2006). Source
119 apportionment techniques - such as positive matrix factorization (PMF) allow for
120 applying thousands of individual species for source identification and the error of
121 analysis to constrain the fitting, and would thus appear more suitable to identify and
122 apportion PM to their sources (Ulbrich et al., 2009). Compared with the number of
123 aerosol source apportionment studies using PMF in Eastern China (e.g., Sun et al., 2013b;
124 Zhang et al., 2013), there were fewer studies in inland cities of China (Elser et al., 2016),
125 the results of which can be used for inter-comparison and understanding the difference of
126 aerosol pollution in different parts of China. In addition, it has been known that a large
127 mass fraction of ambient PM during haze episodes is from fine particles, of which
128 secondary species (some carbonaceous components, sulphate, nitrate, and ammonium)
129 are major components (Zhao et al., 2013). However, the formation and evolution
130 mechanisms of those secondary species were poorly understood which previous models
131 tended to underestimate the secondary species budget in polluted regions (e.g., Volkamer
132 et al., 2006).

133

134 Online instruments based on mass spectrometric techniques, such as Aerodyne aerosol
135 mass spectrometer (AMS) (Jayne et al., 2000), appear to be advance on probing the fast
136 aerosol chemical processes because of the output of a large amount of chemical
137 information and its fine time resolution (in minutes) and mass sensitivity (in ng m^{-3})
138 (Canagaratna et al., 2007). Aerodyne high resolution time-of-flight mass spectrometer
139 (HR-ToF-AMS) have been widely employed for the chemical characterization of
140 submicron aerosol (PM_{10}) (DeCarlo et al., 2006), which provides on-line quantitative mass
141 spectra of the non-refractory (inorganic and organic) aerosol components with high time
142 resolution. Frequently, the organic aerosol (OA) can be further analyzed using the PMF

143 algorithm (Ulbrich et al., 2009; Zhang et al., 2011a), which can represent the organic
144 mass spectral matrix as a set of source/process-related factor mass spectra and time series.
145 In addition, carbon isotope technique has been recently applied to quantify the fossil/non-
146 fossil origins of carbonaceous aerosols, and in combination with AMS-PMF analyses, the
147 assessment of the origin of secondary organic aerosol (SOA) became possible
148 (Minguillon et al., 2011; Huang et al., 2014; Zotter et al., 2014; Beekmann et al., 2015).

149

150 In a previous study, we used an HR-ToF-AMS to investigate the chemical characteristics
151 of PM₁ in the urban area of Lanzhou during summer 2012 (Xu et al., 2014). During that
152 study, organics in PM₁ was found to mainly originate from traffic, cooking activities, and
153 chemical reactions which produced semi-volatile and less-volatility oxygenated OA.
154 Compared to summer situation, energy consumption for heating is huge during winter
155 and the dry and stable meteorological condition in the valley leads to longer aerosol
156 lifetime during winter. Thus aerosols are influenced largely by very different chemical
157 processes between the two seasons. More intensive measurements of PM chemical
158 characteristics are needed to better understand aerosol sources, to quantify their lifetime
159 in the atmosphere and to constrain the uncertainties of their climatic influences. During
160 winter of 2013/2014, we conducted such a study at an urban site of Lanzhou. In this
161 paper, we focus on the chemical speciation of PM₁ and source apportionment of OA.

162

163 **2 Measurement and methods**

164 2.1 Sampling site

165 Aerosol particle measurements were conducted from January 10 to February 4, 2014, at
166 the top floor of a twenty-two story building (~70 m a.g.l) (36.05 °N; 103.85 °W, 1569 m
167 a.s.l) in the campus of Lanzhou University (Fig. S1a). The campus is located in the
168 Chenguan district of Lanzhou which is a cultural and educational area. The twenty-two
169 story building sits at the western edge of the campus and faces a south-northern arterial
170 road (Fig. S1a). At the campus side of this building, there is a three story dining hall of
171 Lanzhou University, and over the arterial road side, there are many restaurants and

172 residents. The room temperature was kept at ~ 20 °C by a central heating radiator. The
173 weather in Lanzhou during the campaign was cold (avg. $T = 0.5$ °C) and dry (avg. RH =
174 28%), and was influenced by the Asian winter monsoon. Because Lanzhou is surrounded
175 by mountains, atmospheric condition is normally stable with low wind speed (on average
176 0.82 m s^{-1} during this study). The sampling site represents a typical urban area dominated
177 by residential and commercial area.

178

179 2.2 Instruments

180 The physiochemical properties of aerosol particles were monitored in real-time by a suite
181 of instruments (Fig. S1b). The sampling inlet, constructed using 0.5 inch copper tube,
182 stemmed out of the rooftop by about 1.5 m. A $\text{PM}_{2.5}$ cyclone (model URG-2000-30EH,
183 URG Corp., Chapel Hill, NC, USA) was used for removing coarse particles. The length
184 of the sampling line was about 5 m. A diffusion dryer was placed upstream of this line to
185 eliminate potential RH effect on particles. The inlet was shared by an Aerodyne HR-ToF-
186 AMS (Aerodyne, Inc., Billerica, MA, USA) for the size-resolved chemical speciation of
187 non-refractory sub-micrometer PM (NR- PM_1), a single particle intra-cavity laser induced
188 incandescence photometer (SP2, DMT, Inc., Boulder, CO, USA) for refractory black
189 carbon (rBC) measurement, a customer-made scanning mobility particle sizer (SMPS)
190 (Wiedensohler et al., 2012) for measuring particle size distribution between 10-800 nm,
191 and a $7\text{-}\lambda$ aethalometer (model AE31, Magee Scientific, Berkeley, CA, USA) to derive
192 the mass concentration of light absorbing black carbon (BC) particles. The total air flow
193 rate from the inlet was $\sim 16 \text{ L min}^{-1}$, with a vacuum pump drawing the air at a flow rate
194 of 10 L min^{-1} and the other 6 L min^{-1} sampled by the instruments. The retention time of
195 particles in the sampling line was less than 2.5 s. A parallel inlet with a 1:10 dilution
196 stage was setup for real-time $\text{PM}_{2.5}$ measurement using a tapered element oscillating
197 microbalance (TEOM series 1400a, R&P, East Greenbush, NY, USA). The roof of the
198 building also hosted instruments for monitoring meteorological parameters such as
199 visibility, air temperature, wind direction, wind speed, and RH. The visibility was

200 measured with a LED-based (880 nm) forward (42 °) scattering visibility sensor (model
201 M6000, Belfort Ins., Maryland, USA).

202

203 2.2.1 HR-ToF-AMS operation

204 A detailed description of the principle and design of HR-ToF-AMS can be found
205 elsewhere (Jayne et al., 2000; DeCarlo et al., 2006). Briefly, HR-ToF-AMS consists of
206 three major sections: the inlet system, the particle sizing vacuum chamber, and the
207 particle composition detection section. The combination of a 100 μm orifice and an
208 aerodynamic lens in the inlet system are used to focus the airborne particles into a
209 concentrated and narrow beam, and then accelerated into the vacuum chamber ($\sim 10^5$
210 Torr) modulated by a chopper for measuring aerodynamic size of the particle; Before
211 being detected, the particles are flash vaporized under 600 °C and ionized by a 70 eV
212 electron impact, and finally detected by the high resolution time-of-flight mass
213 spectrometer. The chopper works at three positions alternately, i.e., an open position
214 which transmits the particle beam continuously, a close position which blocks the particle
215 beam completely, and a chopping position which modulates the beam transmission (2%
216 duty cycle). The open and close positions yield the bulk and background signals for the
217 airborne particle, respectively, while the chopping position modulates the particle beam
218 by spinning chopper wheel (~ 150 Hz) to yield size-resolved spectral signals. The mass
219 spectrometer in the detection section works in two modes based on the ionic path, i.e., V-
220 mode and W-mode, with high sensitivity and high chemical resolution (~ 6000 m/ Δ m),
221 respectively. The highly sensitive V-mode signals are usually used for reporting mass
222 concentration, while the high chemical resolution W-mode signals are used for the
223 analyses of mass spectrum. The time resolution for both V and W modes was 5 min.
224 Under V-mode, the instrument switched between the mass spectrum mode and the PToF
225 mode every 15 s, spending 6 and 9 s on each, and cycled 20 times in one run; No PToF
226 data were recorded in W-mode due to low signal-to-noise (S/N) ratios.

227

228 The instrument was calibrated for ionization efficiency (IE), inlet flow rate, and particle
229 sizes using the standard procedure described by (Jayne et al., 2000). These three
230 calibrations were performed at the beginning, in the middle and end of the field study.
231 Particle-free ambient air was sampled at the end of the study to determine the detection
232 limits (DLs) of individual species and also for adjusting the fragmentation table. Default
233 relative ionization efficiency (RIE) values were assumed for organics (1.4), nitrate (1.1),
234 sulphate (1.2), and chloride (1.3), while an RIE value of 3.9 was determined for
235 ammonium following the analysis of pure NH_4NO_3 . The close concentrations between
236 measured ammonium and predicted ammonium based on the stoichiometric charge
237 balance between nitrate, sulphate, and chloride (slope = 0.94, Fig. S4) suggest that these
238 RIE values are suitable for this campaign.

239

240 2.2.2 Operations of other instruments

241 The SMPS consisting of a condensation particle counter (CPC) (TSI, model 3772) and a
242 differential mobility analyser (DMA) was deployed at 5 min interval. Sample and sheath
243 flow rates of the DMA were set to 1 L min^{-1} and 5 L min^{-1} , respectively. The SMPS was
244 calibrated using a polystyrene latex (PSL) standard prior to field measurements.

245

246 The SP2 uses an intra-cavity Nd:YAG laser at 1064 nm to determine the optical size of a
247 single particle by light scattering and, if material within the particle absorbs at this laser
248 wavelength, the refractory mass of the particle quantified by detection of the main light-
249 absorbing component is rBC. The SP2 incandescence signal was used to obtain single
250 particle rBC mass after calibration with Aquadag standard BC particles. The measured
251 rBC mass is converted to a mass equivalent diameter, which is termed as the BC core
252 diameter (D_c) - the diameter of a sphere containing the same mass of rBC as measured in
253 the particle. Any measured particle with a detectable incandescence signal is referred to
254 as an rBC particle, whereas a particle which only exhibits a scattering signal is termed as
255 a non-BC particle. The total rBC mass loading is reported as the sum of all detected
256 single particle rBC masses.

257

258 The aethalometer measures the optical attenuation (absorbance) of light from LED lamps
259 emitting at seven wavelengths (370, 470, 520, 590, 660, 880, and 950 nm) with a typical
260 half-width of 20 nm. The difference in light transmission through the particle-laden
261 sample spot and a particle free reference spot of the filter is attributed to the absorption
262 caused by aerosol. The attenuation of light is converted to the BC mass concentration
263 using wavelength-dependent calibration factors as recommended by the manufacturer.
264 BC was measured using data at 880 nm using a specific attenuation cross section of 16.6
265 $\text{m}^2 \text{g}^{-1}$ during the campaign. The flow rate was maintained at 4.8 L min^{-1} calibrated using
266 a flow meter. Detection limit of the aethalometer BC was determined to be 0.16–0.28 μg
267 m^{-3} with a flow rate of 4.8 LPM and 5 min time interval, calculated as three times the
268 standard deviation (3σ) of the dynamic blanks. The TEOM was operated at a temperature
269 of 40 °C other than normal operation condition (50 °C) to dry the aerosol in order to
270 minimize mass loss due to volatilization of semi-volatile aerosol compounds. The time
271 resolution of $\text{PM}_{2.5}$ mass concentration was 5 min.

272

273 2.3 Data processing

274 2.3.1 General AMS data processing

275 The HR-ToF-AMS data were processed using the standard software of SQUIRREL
276 (v1.56) and PIKA (v1.15c) ([http://cires.colorado.edu/jimenez-](http://cires.colorado.edu/jimenez-group/ToFAMSResources/ToFSoftware/index.html)
277 [group/ToFAMSResources/ToFSoftware/index.html](http://cires.colorado.edu/jimenez-group/ToFAMSResources/ToFSoftware/index.html)) to determine the mass
278 concentrations and the size distributions of the NR- PM_1 species and the ion-specified
279 mass spectra of organics, written in IGOR (Wavemetrics, Inc., Lake Oswego, OR, USA).
280 An empirical particle collection efficiency (CE) of 0.5 was used, which has been widely
281 used in field studies employing AMS with a dryer installed in front of the equipment's
282 particle inlet. This CE value was further validated by the consistency between HR-ToF-
283 AMS and SMPS data ($R^2 = 0.9$, Slope = 1.48, Fig. S3). The elemental ratios of OA (O:C,
284 H:C, and OM:OC) for this study was determined using the "Aiken ambient" method
285 (Aiken et al., 2008) other than the "improved-ambient" method (Canagaratna et al., 2015)

286 which increased O:C on average by 27%, H:C on average by 10%, and OM:OC on
287 average by 7% (Fig. S2). These "Aiken ambient" results of elemental ratios are more
288 suitable here to allow for comparison with those during summer 2012.

289

290 2.3.2 Positive Matrix Factorization (PMF) analyses

291 The source decomposition of organics was analysed by PMF with the multilinear engine
292 (ME-2) algorithm which serves to reduce rotational ambiguity within the PMF2
293 algorithm. The ME-2 algorithm allows the user to add a priori information into the model
294 (e.g., source profiles) to constrain the matrix rotation and separate the mixed solution or
295 the weak solution. The PMF analysis of organic matrix using ME-2 algorithm is
296 implemented within the toolkit SoFi (Source Finder) and performed by the so-called α -value
297 approach (Canonaco et al., 2013). First, organic matrix was analysed using the PMF2.exe
298 algorithm in robust mode (Paatero and Tapper, 1994) and explored using the PMF
299 Evaluation Toolkit (PET) (Ulbrich et al., 2009). The PMF solution was evaluated
300 following the procedures outlined in Table 1 of Zhang et al. (2011a) including
301 modification of the error matrix and downweighting of low S/N ions. Moreover, based on
302 the AMS fragmentation table, some organic ions were not directly measured but scaled to
303 the organic signal at m/z 44, which were downweighted by increasing their errors by a
304 factor of 3. Some highly polluted periods were deleted during PMF analysis such as
305 January 22-23, 2014. The results of four, five, and six factor solutions with f_{Peak} at 0 are
306 shown in supplementary material (Fig. S5-S7). It is easy to find that a hydrocarbon-like
307 OA (HOA) factor, a cooking-emitted OA (COA) factor, a less-oxidized and more-
308 oxidized OA (LO-OOA and MO-OOA) factors could be clearly separated in the four-
309 factor solution; for the HOA factor, there were significant contributions from m/z 60, 73,
310 91, and 115 in the mass spectrum, suggesting a mixing of multiple sources. In the five-
311 factor solution, a coal combustion-emitted OA (CCOA) factor was separated; however,
312 m/z 60 and 73 which are related to biomass burning OA (BBOA) could not be separated.
313 We then performed OA source apportionment using the ME-2 algorithm by constraining
314 the profiles of HOA and BBOA with the fixed α -value of 0.1 for HOA and 0.4 for BBOA.

315 The a-value test was performed following the technical guidelines presented in Crippa et
316 al. (2014). The reference profile of HOA was adopted from the HOA of the summer
317 study and the reference profile of BBOA was adopted from the nine-factor PMF solution
318 of this study.

319

320 The size distributions of individual OA factors were determined via a multivariate linear
321 regression technique (Ge et al., 2012). This algorithm assumes that each OA mass
322 spectrum is the linear superposition of the mass spectra of individual OA factors, whose
323 mass profiles are constant across the whole size range. Further details about the algorithm
324 can be found in Xu et al. (2014).

325

326 2.3.3 Radiocarbon (^{14}C) data analysis

327 In order to identify the origins of SOA, we conducted ^{14}C analysis on four filter samples.
328 These filter samples were collected at the CAEERI site which is about 500 m away from
329 the LZU site (Fig. S1a). Filter samples were collected using a low volume $\text{PM}_{2.5}$ sampler
330 (16.7 L min^{-1}) during January 2014 with a 24 h sampling time in every week for each
331 filter (January 3rd, 8th, 15th, and 23rd, respectively) on pre-baked quartz filters. One
332 field blank filter was collected and analysed to correct the filter sample measurements.
333 Here, we use the results of these four filter samples to represent the average situation of
334 the field sampling. During the field study period, the air mass and aerosol source are
335 pretty stable which mainly originated from regional sources as illustrated from the
336 consistent variations of chemical composition (section 3.1.3). This can also be evidenced
337 from the relative calm meteorological conditions during the whole sampling period
338 (section 3.1.1). Organic carbon (OC) was separated from the filters by combustion at 375
339 $^{\circ}\text{C}$ during 200 s in pure oxygen in a thermo-optical OC/EC analyser (Model 4L, Sunset
340 Laboratory Inc, USA) (Zhang et al., 2012). The carbon isotopic analysis was conducted
341 by online coupling of the OC/EC analyser with the accelerator mass spectrometry system
342 MICADAS at the University of Bern, Switzerland (Zotter et al., 2014; Agrios et al.,

343 2015). Fossil ^{14}C measurement results were transferred into the non-fossil fraction (f_{NF})
344 of OC using a conversion factor of 1.03.

345

346 For the apportionment of AMS-PMF OA factors using ^{14}C data (Zotter et al., 2014), we
347 assume that all OC sources are represented by the six PMF factors and the f_{NF} in NR-PM₁
348 was the same as that in PM_{2.5}. The OA mass of each PMF factor and total OA were first
349 converted to OC mass using the OM:OC ratios derived from its MS (OM:OC_{HOA} = 1.29,
350 OM:OC_{BBOA} = 1.5, OM:OC_{COA} = 1.27, OM:OC_{CCOA} = 1.37, OM:OC_{LO-OOA} = 1.55,
351 OM:OC_{MO-OOA} = 2.01, OM:OC_{total} = 1.51). For the OC mass concentration of the AMS
352 factors, the following notations, hydrocarbon-like organic carbon (HOC), biomass
353 burning organic carbon (BBOC), cooking organic carbon (COC), coal combustion
354 organic carbon (CCOC), oxygenated organic carbon (OOC), total organic carbon from
355 AMS (TOC_{AMS}), were adopted in the following sections. An f_{NF} value was assumed a
356 priori for the primary PMF factors HOC, BBOC, COC, and CCOC. The average f_{NF} of
357 OOC is then derived by the equation below:

358

$$359 \quad f_{\text{NF_OOC}} = (\text{TOC}_{\text{NF_AMS}} - f_{\text{NF_HOC}} \times \text{HOC} - f_{\text{NF_BBOC}} \times \text{BBOC} - f_{\text{NF_COC}} \times \text{COC} - f_{\text{NF_CCOC}} \\ 360 \quad \times \text{CCOC}) / (\text{SV-OOC} + \text{LV-OOC})$$

361 Here HOC is assumed to originate from gasoline and diesel exhaust and contains
362 exclusively of fossil carbon, i.e., $f_{\text{NF_HOC}} = 0$; BBOC is estimated partly from fossil
363 carbon such as soft coal due to the popular usage in local residents, i.e., $f_{\text{NF_BBOC}} = 1$;
364 COC is assumed to originate from non-fossil carbon such as cooking oil and dressing, i.e.,
365 $f_{\text{NF_COC}} = 1$; CCOC is estimated to originate from coal combustion, i.e., $f_{\text{NF_CCOC}} = 0$.

366

367 3 Results and discussions

368 3.1 Overview of field study

369 3.1.1 Meteorological conditions

370 Fig. 1 shows the time series of meteorological parameters and PM₁ components during
371 January 10–February 4, 2014. During the campaign, the measurement site mainly
372 received air masses from northern and northwestern associated with low wind speeds (on
373 average: $0.8 \pm 0.4 \text{ m s}^{-1}$). The wind directions were associated with the typical
374 anticyclone mesoscale weather forced by Tibetan Plateau in Lanzhou during winter. The
375 mountains to the north and south of the city significantly reduced the wind speed. Air
376 temperature was typical in winter of Lanzhou ranging from -10 to $14 \text{ }^\circ\text{C}$ (average = $0.5 \pm$
377 $5.0 \text{ }^\circ\text{C}$), but was a little warmer after the Chinese New Year (January 31, 2014) (Fig. 1a).
378 No precipitation event occurred during the campaign, and RH was pretty low ranging
379 from 8.8 to 50.7% (avg. = $27.7 \pm 9.1\%$). The visibility ranged from 3.7 to 50 km (avg. =
380 $16.0 \pm 8.7 \text{ km}$).

381

382 3.1.2 Inter-comparisons

383 The inter-comparisons between AMS vs. SMPS and TEOM are shown in Fig. S3.
384 Comparison between the mass concentration of PM₁ and the volume of particle measured
385 by SMPS is tightly correlated ($R^2 = 0.9$) with a slope of 1.48, which represents the
386 average density of bulk particles, assuming that the AMS and the SMPS measure a
387 similar particle population. This value is indeed very close to the estimated PM₁ density
388 (1.46) based on the measured particle composition for this study (using density of 1.2 g
389 m^{-3} for organics, 1.72 g m^{-3} for NH_4NO_3 , 1.77 g m^{-3} for $(\text{NH}_4)_2\text{SO}_4$, 1.52 g m^{-3} for NH_4Cl
390 and 1.8 g m^{-3} for BC) (Zhang et al., 2005; Bond and Bergstrom, 2006). The mass
391 concentration of PM₁ is also closely correlated ($R^2 = 0.71$) with TEOM PM_{2.5}
392 concentrations with a slope of 0.73. Similar contribution of PM₁ to PM_{2.5} were also
393 observed in other cities in China during winter (Elser et al., 2016), such as Beijing (0.74
394 during 2011) (Sun et al., 2013b). Note that the actual mass ratio between PM₁ and PM_{2.5}

395 should be higher than these values since refractory materials such as crustal components
396 were not measured.

397

398 3.1.3 PM₁ composition, variation, and acidity

399 The average mass concentration of PM₁ (NR-PM₁ + BC) was 57.3 μg m⁻³ (ranging from
400 2.1 to 229.7 μg m⁻³ for hourly average) during this study, with 51.2% of organics, 16.5%
401 of nitrate, 12.5% of sulphate, 10.3% of ammonium, 6.4% of BC, and 3.0% of chloride
402 (Fig. 2a). The average mass concentration was more than twice the average value
403 observed during summer 2012 (24.5 μg m⁻³). All species showed similar day-to-day
404 variation with nitrate being the most significant one (Fig. 1e), suggesting an important
405 local source for nitrate. The mass contributions of PM₁ species from low to high PM₁
406 concentrations showed an increased contribution for organics (49% to 53%) and nitrate
407 (13% to 18%), but a decreased contribution for sulphate (17% to 11%) and BC (7.3% to
408 5.3%) suggesting somewhat different chemical processes/sources for each species during
409 the haze pollution (Fig. 2b). Specifically, the increased organics was mainly due to the
410 contribution of primary OA (POA) based on PMF analysis (more discussion are given in
411 section 3.5). During the late part of Chinese New Year holiday (February 3 to end of the
412 study), PM₁ concentration decreased in association with increased wind speed (~1 m s⁻¹
413 to 2 m s⁻¹). NR-PM₁ appeared to be neutralized throughout this study, as indicated by an
414 overall stoichiometric charge balance between the anions (i.e., nitrate, sulphate, and
415 chloride) and the cation ammonium (slope = 0.94, Fig. S4). This result indicates that the
416 inorganic particulate species were mainly present in the forms of NH₄NO₃, (NH₄)₂SO₄,
417 and NH₄Cl in PM₁.

418

419 3.1.4 Size distribution

420 The average chemically-resolved size distributions of NR-PM₁ species are shown in Fig.
421 3a. While all components peaked between 400–500 nm, organic aerosol presented a
422 wider distribution than the inorganics and extended to ~250 nm, suggesting the influence
423 of fresh organics (POA, more discussion are given in section 3.4). These features were

424 similar to those found in most urban sites by the AMS. The similar mode size of
425 inorganics and SOA (Fig. 3c) suggested the well internally mixed air mass during the
426 sampling period. The mass contributions of chemicals at the major peak (400–500 nm)
427 were organics (~50%), nitrate (~20%), ammonium (~15%), sulphate (~10%), and
428 chloride (~5%); while the contribution of organics increased with the decreasing of size
429 mode (Fig. 3c). Comparing with the results observed during 2012 summer, the size
430 distributions of aerosol particle during winter were narrower, although the mode sizes of
431 major peaks were similar, indicating highly mixed and aged aerosol particles during
432 winter.

433

434 3.2 Diurnal variations of aerosol species

435 All species show significant diurnal variations during the study suggesting the important
436 local and regional sources of aerosol (Fig. 4). The observed diurnal trends of BC
437 presented two dominant peaks with one at late morning (10:00–12:00) and another at
438 early evening (20:00–22:00). The morning peak did not overlap with the rush hours
439 (7:00–9:00), different than that of summer 2012; the BC mass loading started to increase
440 from 6:00 continuously during morning, and reached maximum between 10:00–12:00
441 and then dropped down after the noon time. Another combustion tracer, carbon monoxide
442 (CO), also showed the similar morning peak (Fig. 5). This morning peak was likely
443 resulted from the formation of inversion layer during winter at Lanzhou which promoted
444 accumulation of air pollutants from enhanced human activities in the morning. This
445 inversion layer frequently formed from night time and diffused after the noon time due to
446 the valley terrain (Zhang et al., 2011b). The temperature profile observed at the suburban
447 Lanzhou (Yuzhong, ~30 km from the sampling site) showed a strong inversion in the low
448 boundary layer during the morning time (Fig. S8). The evening peak of BC could result
449 from increased human activities such as traffic, cooking, and heating coupled with low
450 boundary layer after sunset. Organics had two sharp peaks at the noon time (12:00–13:00)
451 and early evening (19:00–20:00) which correspond to lunch time and dinner time,
452 respectively, indicating the importance of cooking-related emissions of OA. PMF

453 analysis show that cooking-emitted aerosol could contribute up to 30 – 60% of organics
454 during meal times (section 3.4.3).

455

456 Sulphate presented two peaks with one occurring at the noon time (11:00–14:00) in
457 accordance with the photochemical processes; this peak is narrower than that during
458 summer, likely due to relatively weak photochemical activities. Another minor peak
459 occurred between 20:00–22:00 which was likely due to the lowered boundary layer depth.
460 The significantly higher concentration of sulphate during winter than summer could
461 result from a higher precursor SO₂ emission and stagnant atmospheric conditions in
462 winter. The diurnal pattern of sulphate during winter was similar to that of summer 2012
463 at Lanzhou and summer 2011 at Beijing, but was different from that of Beijing during
464 winter 2011/2012 where aqueous processing was found to could play an important role
465 (Sun et al., 2013b). Chloride had similar diurnal pattern with sulphate, although the
466 evening peak was more obvious. The major source of hydrochloric acid is biomass
467 burning, coal combustion and waste combustion (Ianniello et al., 2011). The significant
468 evening peak could be related with these sources coupled with the shallow boundary
469 layer. The high background concentrations of chloride during day and night suggest a
470 persistent emission of hydrochloric acid which could be from the heating factory and
471 power plants. The diurnal pattern of chloride during winter was different from that during
472 summer 2012 which peaked during the night time due to temperature-dependent gas-
473 particle partitioning. Nitrate peaked between 12:00–16:00, right after the peak of sulphate.
474 The formation of nitrate during afternoon suggests that nitrate was dominated by the
475 homogeneous photochemical production. Fig. 5 shows the variations of NO_x and O₃
476 calculated from data downloaded from one station monitored by the Ministry of
477 Environmental Protection of China, ~3 km southwest of sampling site (Fig. S1a); NO had
478 a morning peak (7:00–10:00) and an evening peak (19:00–21:00) corresponding to rush
479 hours; NO₂ increased from 10:00 which formed from NO consumed by OH radical and
480 slightly decreased from 14:00 to 18:00 corresponding to the formation of nitrate and O₃
481 during afternoon. The diurnal change of NO_x (Δ NO_x) mixing ratio was ~50 ppbv (from
482 150 to 100 ppbv), while the diurnal change of the sum of Δ O₃ and Δ NO₃⁻ was ~30 ppbv.

483 Considering the higher mixing layer height during afternoon, it seems that nitrate was
484 mainly formed from the photochemical processing of NO_x. The diurnal pattern of nitrate
485 during winter was vastly different from that during 2012 summer which was mainly
486 controlled by the dynamic of mixing layer and gas-particle partitioning. It seems that,
487 from the diurnal variation, atmospheric ammonia was first neutralized by sulphuric acid
488 and hydrochloric acid to form ammonium sulphate and ammonium chloride, and the
489 remaining ammonia may then combine with nitric acid to form ammonium nitrate.

490

491 3.3 Bulk characteristics and elemental ratios of OA

492 Table 1 shows the average elemental mass composition and mass contributions of six ion
493 categories to the total organics. Carbon contributed 66% to the organics following by
494 oxygen (25%), hydrogen (8%), and nitrogen (1%); correspondingly, C_xH_y⁺ dominated the
495 organics by 59%, following by C_xH_yO₁⁺ (26%), C_xH_yO₂⁺ (10%), H_yO₁⁺ (2%), and
496 C_xH_yN_p⁺ (2%). Compared with the results of 2012 summer, the organics in winter had
497 higher carbon (66% *vs.* 59%) and C_xH_y⁺ content (59% *vs.* 56%), and lower oxygen
498 content (25% *vs.* 26%) (Fig. 6c); this suggests that the organics during winter had a
499 higher fraction of primary compounds than those during summer which was likely due to
500 weaker photochemical activities, lower boundary layer height and more emissions from
501 primary sources. The average O/C of organics, an indicator for oxidation state, was 0.28
502 during this study which was somewhat lower than that of summer 2012 (0.33) (Fig. 6a
503 and b). Photochemical processing of organics during winter appeared to be significantly
504 weaker and shorter than those during summer as shown by the smaller diurnal peak of
505 O/C (Fig. 6d). The diurnal profile of H/C was inversely correlated with that of O/C, and
506 the peaking of organic aerosol concentration usually corresponded to the high H/C ratio
507 and low O/C ratio, indicating the dominant role of primary OA.

508

509 3.4 Source apportionment of OA

510 Source apportionment via PMF with ME2 engine on OA mass spectra resolved six
511 components, i.e., HOA, COA, CCOA, BBOA, LO-OOA, and MO-OOA. Each

512 component has a unique mass spectral pattern, diurnal pattern, and temporary variation
513 which correlated with corresponding tracers such as inorganic species. Two OOA
514 components can be regarded as surrogates of secondary OA (SOA), with MO-OOA for
515 more aged SOA and LO-OOA for fresher SOA; The HOA, BBOA, COA and CCOA
516 components are regarded as primary OA (POA) based on their low O/C ratios and good
517 correlations with primary aerosol tracers (Fig. 7). Comparison with the source
518 apportionment results of summer 2012, the organic sources and chemical processes
519 during winter 2013/2014 were more complex due to the multiple primary sources.
520 Detailed discussion of each factor is given in the following subsections.

521

522 3.4.1 HOA

523 HOA factors had been frequently separated from the OA in urban area due to the
524 emission from traffic and/or other fossil combustion activities (e.g., Sun et al., 2011b; Ge
525 et al., 2012). The diurnal pattern of HOA in winter 2013/2014 of Lanzhou shows two
526 predominant peaks in the morning (10:00–12:00) and evening (20:00–21:00),
527 respectively (Fig. 5). The morning peak started from 6:00 was mainly associated with the
528 morning traffic rush hours, and it maximized at late morning associating with the
529 inversion layer as discussed in Section 3.2. The evening peak was relevant with the
530 evening rush hours and low PBL depth after sunset. The relatively low concentration
531 during afternoon was probably due to the high PBL depth as shown by the mass
532 concentration variations of BC. The correlation between HOA and BC was high ($r = 0.84$,
533 Fig. 7f and Table 2), as a big fraction of BC has been thought to emit from traffic
534 activities and commonly used as a tracer of traffic emission. The minimum of HOA
535 concentration, which typically occurred during afternoon or middle night, was still up to
536 $\sim 2 \mu\text{g m}^{-3}$ suggesting a high background of HOA which is likely due to the stagnant air
537 condition unfavourable for the diffusion of aerosol. The size distribution of HOA showed
538 a mode size of $\sim 200 \text{ nm}$ (Fig. 3b) corresponding to the primary emitted aerosol
539 behaviours and HOA could account for $\sim 25\%$ mass of aerosols between 100-300nm (Fig.
540 3c). The average concentration of HOA during 2013/2014 winter was $2.6 \mu\text{g m}^{-3}$

541 accounting for 9% of organics (Fig. 8a). This concentration was higher than that of 2012
542 summer in Lanzhou (2.6 vs. 1.8 $\mu\text{g m}^{-3}$) likely due to the lower PBL during winter and
543 stagnant air conditions. The mass contribution from HOA is similar to the result of 2013
544 winter at Beijing (9%) which was also the lowest contributor to the total OA (Sun et al.,
545 2013b; Zhang et al., 2014), probably due to more modern vehicles were used in the recent
546 years.

547

548 3.4.2 BBOA

549 BBOA component had been widely observed in USA and European countries during
550 winter due to the traditional wood burning for residential heating (Alfarra et al., 2007).
551 The BBOA component is thought to be less important in China because coal is the major
552 fuel during winter. BBOA could be an important component in China during some
553 special periods. For example, Zhang et al. (2015a) identified a BBOA factor in urban
554 Nanjing, southeast of China, during harvest seasons of summer and autumn because of
555 the burning of straw. The BBOA component has also been identified in some regions in
556 China where the coal resource is scarce. For example, Du et al. (2015) separated a BBOA
557 factor at a rural site of the northern Tibetan Plateau due to the widely usage of cow dung
558 cake for heating in this region. The BBOA component has also been identified during
559 winter in cities in southern China because of rich wood resource in these regions (He et
560 al., 2011; Huang et al., 2011; Huang et al., 2013). To our knowledge, only two recently
561 papers have reported the identification of a BBOA factor during winter using online
562 measurement in an urban area of northern China (Elser et al., 2016). Although the high
563 contribution of non-fossil carbonaceous aerosol was found (Zhang et al., 2015b) and the
564 mass spectra of organic in other cities (such as Beijing) during winter have also
565 significant contributions from m/z 60 and 73 (Sun et al., 2013b; Zhang et al., 2014), it is
566 difficult to separate the BBOA using general PMF because of its similar temporal
567 variation with CCOA, such as diurnal pattern (Fig. 4). BBOA contributions presented a
568 clear periodic change (Fig. 1), and on average were high during night time and low
569 during daytime (Fig. 5). This trend is consistent with conventional usage of biomass for

570 heating. The time series of BBOA was also closely correlated with BC and chloride
571 (Table 2) due to significant emission of these species from biomass burning. The average
572 mass concentration of BBOA was $3.2 \mu\text{g m}^{-3}$, on average contributing 11% of the total
573 OA mass for the entire study (Fig. 8a), but could reach up to 20% during night and down
574 to less than 5% during afternoon (Fig. 8b). This average concentration was close to the
575 results observed at southern Chinese cities such as Jiaying ($\sim 3.9 \mu\text{g m}^{-3}$) (Huang et al.,
576 2013), Kaiping ($\sim 1.36 \mu\text{g m}^{-3}$) (Huang et al., 2011) and Shenzhen ($\sim 5.2 \mu\text{g m}^{-3}$) (He et
577 al., 2011).

578

579 The size distribution of BBOA peaked at $\sim 400\text{nm}$ which is close to accumulation mode
580 (Fig. 3b). This feature could be due to internal mixing or coagulation of particles. The
581 O/C ratio of BBOA is 0.26, which is consistent with the primary BBOA feature (Ortega
582 et al., 2013). The similar O/C and the dominance of an accumulation mode in the size
583 distribution of BBOA were also observed during winter in Fresno, a major city in the
584 Central Valley of California, USA (Ge et al., 2012; Young et al., 2015).

585

586 3.4.3 COA

587 The COA component has been widely identified in urban AMS studies and observational
588 results by other instruments recently, and it is regarded as important source of OA in
589 urban areas (Abdullahi et al., 2013 and references therein). The MS of COA in this study
590 had a major contribution from C_xH_y^+ ions (79.7%) with also an important contribution
591 from $\text{C}_x\text{H}_y\text{O}_1^+$ ions (15.5%), similar as those in HOA (80.6% and 13.7%) (Fig. S9). In
592 comparison with the HOA spectrum, COA had a higher m/z 55 to 57 ratio (2.1 vs. 0.7)
593 (Fig. 7) which had been postulated as a significant indicator for COA (Sun et al., 2011b;
594 Mohr et al., 2012). In the V-shape plot defined by Mohr et al. (2012), which uses f_{55} vs.
595 f_{57} after subtracting the contributions from factors of OOA, CCOA, and BBOA (denoted
596 as OOA_CCOA_BBOA_sub , i.e. $f_{55_{\text{OOA_CCOA_BBOA_sub}}}$ and $f_{57_{\text{OOA_CCOA_BBOA_sub}}}$), the
597 data can be clearly represented with ones during morning close to HOA line and ones
598 during meal times close to COA line (Fig. S10). The MS of COA is highly similar to that

599 of summer 2012 observation ($R^2 = 0.95$, slope = 0.97, Fig. S11) which was found to
600 resemble closely the COA MS from other locations (Xu et al., 2014). In fact, the COA
601 components were found to be associated with heating of cooking oils rather than burning
602 of meat/food itself, and indeed the COA mass spectra from cooking of different dishes
603 were highly similar (He et al., 2010). The O/C and H/C ratios of COA were 0.09 and 1.71,
604 respectively, suggesting its feature as POA. This O/C ratio was slightly lower (0.09 vs.
605 0.11) and the H/C was slightly higher than that of 2012 summer (1.71 vs. 1.69). The size
606 distribution of COA was also peaking between 100–200 nm similar to that of HOA (Fig.
607 3b). The diurnal variation of COA displayed two predominant peaks standing out at lunch
608 time (12:00–13:00) and dinner time (19:00–20:00), respectively (Fig. 5), and a small
609 breakfast peak (~8:00). This pattern was consistent with that of summer 2012 (Fig. 4)
610 which resulted from the consistent routine life during winter and summer. The enhanced
611 COA concentration at dinner time might be mainly due to the low PBL height and the
612 activity of a formal meal with more attendants and longer time than that of lunch. The
613 temporal variation correlated tightly with $C_6H_{10}O^+$ ($R^2 = 0.95$, Fig. 8d) which has been
614 reported as the high resolution mass spectral markers for ambient COA (Sun et al., 2011b;
615 Ge et al., 2012).

616

617 The average contribution of COA to organics was 20% (~10–50%) (Fig. 8a) with an
618 average mass concentration of $5.86 \mu\text{g m}^{-3}$ which was much higher than those of HOA
619 and BBOA. This contribution is similar to those in Beijing during winter (average 19% of
620 OA with a range of 16–30%) (Sun et al., 2013b), Fresno (~19% of OA) (Ge et al., 2012),
621 Barcelona (17% of OA) (Mohr et al., 2012), and Paris (11–17%) (Crippa et al., 2013).
622 This high fraction indicates that COA is an important local source of OA in Lanzhou
623 regardless of clear or hazy periods (section 3.5).

624

625 3.4.4 CCOA

626 A CCOA component had been identified in this study with its MS similar to the OA from
627 coal burning in lab study (Dall'Osto et al., 2013). The MS of CCOA had high signals at

628 m/z 41, 43, 44, 55, 57, 69, 91 and 115 (dominated by $C_xH_y^+$ ions) (Fig. 7i) (Elser et al.,
629 2016). $C_xH_y^+$ ions in total account for 75.3% of CCOA MS, following by $C_xH_yO_1^+$
630 (14.7%) and $C_xH_yO_2^+$ (9.4%). The fractions of $C_xH_y^+$ and $C_xH_yO_1^+$ were similar with
631 those in HOA MS (Fig. S9), but the CCOA MS had high signal intensity at m/z 44
632 (mainly CO_2^+) which is different from that of HOA (Fig. 7). This high CO_2^+ fraction was
633 also observed in CCOA MS in Changdao island in China during winter (Hu et al., 2013).
634 Wang et al. (2015) suggested this high CO_2^+ signal is from the oxidative transformation
635 of the pyrolysis products during coal burning. Zhang et al. (2008) reported that 48–68%
636 of particulate organic matter from coal combustion aerosol is found in the form of
637 organic acids. The O/C ratio is thus higher than that of HOA (0.17 vs. 0.10) with a lower
638 H/C ratio (1.67 vs. 1.73). The CCOA also locates in a relatively high and left position in
639 the triangle plot defined by Ng et al. (2010) (Fig. 13a). These features indicate CCOA is a
640 POA factor but is a little more oxygenated than HOA. The time-dependent concentrations
641 of CCOA correlated with BC ($r = 0.74$) and chloride ($r = 0.62$) which also correlated well
642 with HOA and BBOA (Table 2). The CCOA mass loading remained high from 20:00 to
643 10:00, slowly decreased to a minimum at 16:00, and then increased from 16:00 to 20:00
644 (Fig. 5). This diurnal pattern was similar to that of BBOA which were all mainly emitted
645 from heating. The slower decreasing rate during morning and increasing rate during late
646 afternoon for CCOA than those of BBOA could related with wide usage of coal, such as
647 cooking and power plants. In our summer 2012 observation, we also observed OA signals
648 from coal combustion which suggest persistent emitted during the whole year in Lanzhou.
649 The size distribution of CCOA peaked ~ 450 nm (Fig. 3b), similar with that of BBOA.

650

651 The average CCOA mass concentration was $5.3 \mu\text{g m}^{-3}$, accounting for 18% of total OA
652 mass (Fig. 8a). The mass fraction of CCOA could reach to 25% of OA during night and
653 decreased to 3% during afternoon (Fig. 8b). This indicates that CCOA was an important
654 OA component similar as that in Beijing OA (15–55%) (Zhang et al., 2014; Elser et al.,
655 2016), but its mass fraction of $PM_{2.5}$ ($\sim 9\%$) was at the low end of the values observed at
656 Beijing and Xi'an (9–21%) (Huang et al., 2014).

657

658 3.4.5 LO-OOA and MO-OOA

659 Two or more OOA components are commonly separated by PMF in urban areas which
660 correspond to fresh SOA and aged SOA (Jemenez et al., 2009), and the MS of SOA
661 factors all have predominant contributions at m/z 43 and 44. The MS of fresher SOA such
662 as LO-OOA has higher contribution at m/z 43 (mainly $C_2H_3O^+$, accounting for 73% of
663 m/z 43 in this study), while aged SOA such as MO-OOA has higher signal at m/z 44
664 (mainly CO_2^+ , accounting for 98% of m/z 44 in this study). The contribution of $C_xH_yO_1^+$
665 in LO-OOA was 35.6% followed by $C_xH_y^+$ (50.1%), $C_xH_yO_2^+$ (9.4%), $H_yO_1^+$ (1.4%),
666 $C_xH_yN_p^+$ (3.0%), and $C_xH_yO_zN_p^+$ (0.4%) (Fig. S9). The O/C ratio of LO-OOA was 0.31
667 and H/C was 1.47 consistent with fresh SOA. The MS of MO-OOA was comprised of
668 22.1% of $C_xH_yO_2^+$, 35.6% of $C_xH_yO_1^+$, 34.5% of $C_xH_y^+$, 5.5% of $H_xO_1^+$, 2.0% of $C_xH_yN_p^+$,
669 and 0.4% of $C_xH_yO_zN_p^+$ (Fig. S9). The O/C and H/C ratios of MO-OOA were 0.67 and
670 1.29, respectively. Compared with those of summer 2012, both O/C and H/C ratios of
671 LO-OOA during winter 2013/2014 were higher (0.31 vs. 0.28 for O/C, 1.47 vs. 1.34 for
672 H/C), while they were both slightly lower for MO-OOA (0.67 vs. 0.68 for O/C and 1.29
673 vs. 1.34 for H/C). These results indicate that the atmospheric oxidation capacity during
674 winter was still very strong. The positions of LO-OOA and MO-OOA in triangle plot of
675 fCO_2^+ vs. $fC_2H_3O^+$ are situated in the space of triangle plot with MO-OOA at the upper
676 left corner (Fig. 13b) and LO-OOA at the lower right space, respectively, suggesting the
677 different oxidation degree of OOA factors. The MS of LO-OOA and MO-OOA were
678 similar with those of summer 2012 ($R^2 = 0.98$ for MO-OOA and $R^2 = 0.77$ for LO-OOA,
679 Fig. S11). Note that the $C_xH_y^+$ ions in LO-OOA were mainly from by m/z 39, 41, 91 and
680 115 (Fig. 7h), which were also found to be enriched in coal combustion organic aerosols.
681 This feature is similar to that of summer 2012, potentially suggesting that part of LO-
682 OOA was from further oxidation of CCOA.

683

684 The temporal variations of LO-OOA and MO-OOA were highly correlated with
685 secondary inorganic species: LO-OOA vs. sulphate ($R^2 = 0.79$) and MO-OOA vs. nitrate

686 ($R^2 = 0.71$) (Fig. 7a and b, Table 2). These patterns are somewhat contradictory to
687 previous AMS findings that LO-OOA typically correlates better with nitrate due to their
688 similar semi-volatile characteristics while MO-OOA tends to correlate better with
689 sulphate as they are both low-volatility species. These correlations were indeed observed
690 during the summer study of 2012 (Xu et al., 2014). The behaviours of the two OOA
691 factors during this study were likely due to the low air temperature and low RH
692 conditions which favoured nitrate formation primarily through photochemical reactions.
693 This phenomenon was also observed in winter time of Beijing (Sun et al., 2013b).

694

695 The diurnal variation profiles of LO-OOA and MO-OOA all showed one bump with the
696 LO-OOA peaking between 11:00–14:00 and MO-OOA peaking between 12:00–18:00,
697 suggesting the importance of photochemical processes for both OOA factors. The size
698 distribution of the OOA (LO-OOA + MO-OOA) had a mode size of ~550 nm (Fig. 3b)
699 reflecting the feature as SOA. This size mode is slightly bigger than those of OOA in
700 other studies such as Fresno (460 nm) and Lanzhou summer 2012 (~450 nm) likely due
701 to the high concentration of gas precursors and longer lifecycle of aerosol during winter.

702

703 The mass concentrations of LO-OOA and MO-OOA were 7.0 and 5.6 $\mu\text{g m}^{-3}$ with the
704 mass contributions of 24% and 19% to OA, respectively (Fig. 8a). These contributions
705 were lower than those during summer 2012 in Lanzhou (27% for LO-OOA and 32% for
706 MO-OOA) especially for MO-OOA, likely due to the relative weak solar radiation during
707 winter and more primary sources in winter. The diurnal total contribution of OOA (LO-
708 OOA + MO-OOA) varied between 40%–70% (Fig. 8b), suggesting the importance of
709 SOA in the air pollution throughout the day at Lanzhou.

710

711 3.5 Primary and secondary OA

712 As shown in Fig. 2b, the mass fraction of organics increased with the increase of PM_{10}
713 concentration, so it is important to know the relative contributions of primary and

714 secondary OA components during the pollution periods. Fig. 9a shows the scatter plot of
715 SOA (= LO-OOA + MO-OOA) and POA (= HOA + BBOA + COA + CCOA) during this
716 study. It is clear that POA and OOA show correlation during the periods of POA less
717 than $\sim 15 \mu\text{g m}^{-3}$ associated with low mass fractions of OA. When POA and OA fraction
718 increased significantly, POA and OOA show almost no correlation, indicating the
719 importance of POA in the severe aerosol pollutions in Lanzhou during winter. This is
720 different than the observation from summer 2012, during which SOA had a stable
721 contribution to PM_{10} (Fig. 9b), due to more complex POA sources and larger contributions
722 from these sources to PM_{10} mass loading during winter compared to summer. This is even
723 more evident when comparing each POA factor with OA (Fig. 10). The COA had the
724 biggest contribution to the increased organics can explained 59% of the increase of
725 organics, followed by HOA (28%). The components of CCOA and BBOA also had
726 positive contributions to the increase of PM_{10} mass. However, both OOA components had
727 negative slopes with organics with LO-OOA being the major one. The phenomenon of
728 POA dominating during haze periods is different from the results in other cities in China
729 (Huang et al., 2014). For example, Elser et al. (2016) found significant increased
730 contribution from SOA and secondary inorganic aerosol during haze periods in
731 2013/2014 winter in Xi'an and Beijing. This is likely due to the higher RH values in the
732 eastern China which is more favourable for the aqueous-phase production of SOA.
733 Indeed, Sun et al. (2013a) observed significant increase of secondary inorganic aerosol
734 during high RH periods in Beijing.

735

736 The average contribution of POA to organics decreased from 60.0% to 39.3% during
737 Chinese New Year festival of 2014 (Fig. 1) due to the reduced primary aerosol sources
738 (many restaurants were closed during the holiday of Chinese New Year) such as HOA
739 (9.8% to 3.3%), COA (21.1% to 11.6%), CCOA (18.2% to 15.4%), and BBOA (10.8% to
740 9.0%). This is an indication that control of cooking activities and traffic emissions in this
741 residential area may be effective strategies for air quality improvement during winter.

742

743 3.6 Fossil and non-fossil OC

744 OC measured by OC/EC analyser on two filters (OC_{filter}) and corresponding AMS
745 (OC_{AMS}) online measured results are shown in Fig. 11a. The average ratio of
746 $OC_{\text{AMS}}/OC_{\text{filter}}$ was ~ 1.5 for these two filters likely due to the analytical uncertainties of
747 different instruments (30% for AMS and 20% for OC_{filter}), which was also observed in
748 other studies (Zotter et al., 2014). The data from the ^{14}C measurement for the filter
749 samples are listed in Table S1. The total average of f_{NF} in these four filters was $55 \pm 3\%$,
750 with 54% and 57% for filters during Jan. 15 and Jan. 23, respectively. Comparison with
751 other studies, the average f_{NF} value in this study was lower than those in Xi'an (63%) and
752 Guangzhou (65%), and higher than those in Beijing (42%), while similar with those in
753 Shanghai (51%) during 2012/2013 winter (Zhang et al., 2015b). Combining with the f_{NF}
754 value (the total average of f_{NF} for the total average AMS results) and the contributions of
755 fossil (F) POC (HOC and CCOC) and non-fossil (NF) POC (BBOC and COC), the f_{F} and
756 f_{NF} for SOC could be obtained (Fig. 11b). The average f_{F} and f_{NF} for POC and SOC are
757 summarized into Fig. 12. The f_{F} and f_{NF} for POC during Jan. 15 were 47% and 53%,
758 while for SOC were 44% and 56%. For all AMS data, the f_{F} and f_{NF} in POC were 47%
759 and 53%, while for SOC were 42% and 58%. The F-POC during Jan. 15 was comprised
760 by 21% HOC and 26% CCOC, and NF-POC by 16% BBOC and 37% COC. For all AMS
761 data, the F-POC was comprised by 16% HOC and 31% CCOC, and NF-POC by 17%
762 BBOC and 36% COC.

763

764 3.7 Evolution of OA and relationship between odd oxygen and SOA

765 The evolution of OA chemical composition upon aging has been an important subject
766 which is used to understand the formation of SOA. The methods to characterize this
767 evolution include the application of several specific diagrams, such as the AMS triangle
768 plot (f_{44} vs. f_{43} or $f_{\text{CO}_2^+}$ vs. $f_{\text{C}_2\text{H}_3\text{O}^+}$) (Ng et al., 2010). f_{44} is a tracer for aged OA
769 (mostly CO_2^+), while f_{43} (mostly $\text{C}_2\text{H}_3\text{O}^+$, with some contribution from C_3H_7^+) is mainly
770 associated with freshly formed SOA and POA. POA factors are usually located towards
771 the lower and lower-left corner in triangle plot, and with the aging, move up toward the

772 region of LO-OOA indicating by the increased f_{43} and f_{44} ; and with further aging, OA
773 move toward the region of MO-OOA indicating by the increased f_{44} and decreased f_{43} .
774 In the plot of f_{44} vs. f_{43} of this study (Fig. 13a), the data distributed in a narrow space
775 and move up vertically in the triangle space suggesting significant increasing in f_{44} . The
776 data from the low (night time) to the high (afternoon time) f_{44} value corresponded to the
777 evolution of the photo radiation intensity suggesting the photochemical processes. The
778 MO-OOA lay at the top of the data consistent with its highly oxidized feature, while
779 BBOA, COA, and HOA all lay at the bottom of triangle space. CCOA is above those of
780 other primary factors consistent with the results of high acid contents in coal burning OA.
781 In the plot of $f_{\text{CO}_2^+}$ vs. $f_{\text{C}_2\text{H}_3\text{O}^+}$ (Fig. 13b), most of data moved out of triangle space
782 because of the high contribution of C_3H_7^+ at m/z 43, especially for data during night time.
783 $f_{\text{CO}_2^+}$ and $f_{\text{C}_2\text{H}_3\text{O}^+}$ both increased before the noon time, after that $f_{\text{C}_2\text{H}_3\text{O}^+}$ stopped at
784 ~ 0.05 and $f_{\text{CO}_2^+}$ kept increase likely suggesting the evolution of LO-OOA to MO-OOA.
785 In comparison to the results in summer 2012, the data in winter were more concentrated
786 in the triangle space suggesting air masses with similar source contribution during winter.

787

788 In order to understand the possible sources of oxygenated OA, we also compared the
789 diurnal variations between MO-OOA and O_x (Fig. 13c). Both O_x and OOA are products
790 of photochemical reactions and the comparison between O_x and OOA can offer insight
791 into the formation of OA due to the dependence of the ratio on the VOC species
792 (Herndon et al., 2008), assuming aqueous processing and night time oxidation for OOA
793 were less important, such as during this study due to the low RH. High SOA vs. O_x slopes
794 were observed (larger than $0.12 \mu\text{g m}^{-3} \text{ppb}^{-1}$) where aromatic VOC dominated the
795 photochemical processing, while a low slopes ($\sim 0.03 \mu\text{g m}^{-3} \text{ppb}^{-1}$) were observed where
796 alkene VOCs dominated the photochemical processing (Wood et al., 2010; Hayes et al.,
797 2013). Fig. 13c shows the scatter plot between O_x and MO-OOA and sized by the mass
798 concentration of BBOA. O_x and MO-OOA showed tight correlation ($R^2 = 0.9$) with a
799 slope of $0.18 \mu\text{g m}^{-3} \text{ppb}^{-1}$. This result is similar with that found in Beijing during
800 wintertime, which has suggested that semivolatile VOCs (e.g., PAHs) could be the
801 primary precursor of OOA (Hu et al., 2016). Several studies suggested that aromatic

802 VOC is dominant among VOCs in northern China (Zhang et al., 2015c) and can be
803 important contribution for SOA production (Liu et al. 2012). We also did correlation
804 between LO-OOA and Ox, and found the different synchronization of LO-OOA and Ox
805 (Fig. S12). It seems LO-OOA varied two to three hours earlier than Ox, likely suggesting
806 other origination for LO-OOA such as down mixing of mixing-layer aerosol, which is a
807 popular phenomenon in the mountain-valley city (Chen et al., 2009).

808

809 **4 Conclusions**

810 In order to understand the sources and chemical processes of the air pollution during
811 winter in Lanzhou, a field study was conducted at an urban site of Lanzhou during
812 January 10 – February 4, 2014 using a suit of on-line instruments. The results show that
813 the average mass concentration of PM₁ (NR-PM₁ + BC) was 57.3 μg m⁻³ (ranging from
814 2.1 to 229.7 μg m⁻³ for hourly averages), with 51.2% of organics, 16.5% of nitrate,
815 12.5% of sulphate, 10.3% of ammonium, 6.4% of BC, and 3.0% of chloride. This mass
816 concentration was about two times higher than that during summer 2012 in Lanzhou,
817 however, the mass loading levels and chemical compositions were similar to those
818 observed in Beijing during winter. The mass concentration of nitrate and organics
819 increased with the increase of PM₁ loading, while sulphate decreased, indicating the
820 importance of OA and nitrate during severe air pollution. The size distributions of all the
821 species displayed a moderate size at 400–500 nm, suggesting that aerosol particles were
822 largely internally mixed during winter. All species presented significant diurnal
823 variations. BC had two peaks at 10:00–12:00 and 20:00–22:00, respectively. Further
824 analysis indicated that the first peak was resulted from the inversion layer during morning
825 which accumulated the air pollutants from early morning and until the break-up at around
826 noon time. The evening peak of BC was related to human activities such as traffic and
827 coal combustion coupled with the shallow PBL. OA presented two peaks corresponding
828 to lunch and dinner time suggesting cooking to be an important source. Sulphate peaked
829 during the noon time (11:00–14:00) indicating the importance of photochemical
830 processes. Nitrate presented an afternoon peak (12:00–16:00) which indicate the

831 photochemical processing of NO_x. The diurnal pattern of nitrate during winter time was
832 significant different from that during summer 2012 which was thought mainly from the
833 mixing down of aloft residual layer. PMF analysis of organic mass spectrum with the
834 ME-2 engine identified six organic aerosol sources: i.e., HOA, BBOA, COA, CCOA,
835 LO-OOA, and MO-OOA. POA, which includes HOA, BBOA, COA, and CCOA,
836 accounted for 57% of OA mass and showed an increased in concentration with the
837 increase of PM₁ loading. This is an indication that POA emission was one of the main
838 reasons for the occurrence of heavy air pollution episodes. The temporal profile of MO-
839 OOA tightly correlated with that of nitrate, while those of LO-OOA with sulphate
840 correlated. This observation was different than those observed during other studies and
841 during summer at Lanzhou, indicating the importance of photochemistry for nitrate
842 during winter in Lanzhou due to cold air temperature and low RH conditions. ¹⁴C
843 analysis of OOC indicated that 57% of the SOC was formed from non-fossil source.

844

845 **Acknowledgements**

846 The authors thank their colleagues for continuing support and discussion. This research
847 was supported by grants from the Chinese Academy of Sciences Hundred Talents
848 Program, the Key Laboratory of Cryospheric Sciences Scientific Research Foundation
849 (SKLCS-ZZ-2015-01), the National Natural Science Foundation of China Science Fund
850 for Creative Research Groups (41121001, 21407079, 91544220), and the Chinese
851 Academy of Sciences Key Research Program (KJZD-EW-G03).

852 **References**

853

854 Abdullahi, K. L., Delgado-Saborit, J. M., and Harrison, R. M.: Emissions and indoor
855 concentrations of particulate matter and its specific chemical components from
856 cooking: A review, *Atmos. Environ.*, 71, 260-294,
857 doi:10.1016/j.atmosenv.2013.01.061,2013.

858 Agrios, K., Salazar, G. A., Zhang, Y. L., Uglietti, C., Battaglia, M., Luginbühl, M.,
859 Ciobanu, V. G., Vonwiller, M., and Szidat, S.: Online coupling of pure O₂
860 thermo-optical methods - ¹⁴C AMS for source apportionment of carbonaceous
861 aerosols study, *Nucl. Instrum. Meth. Phys. Res. B.*, 361, 288-293,
862 doi:10.1016/j.nimb.2015.06.008, 2015.

863 Aiken, A. C., DeCarlo, P. F., Kroll, J. H., Worsnop, D. R., Huffman, J. A., Docherty, K.
864 S., Ulbrich, I. M., Mohr, C., Kimmel, J. R., Sueper, D., Sun, Y., Zhang, Q.,
865 Trimborn, A., Northway, M., Ziemann, P. J., Canagaratna, M. R., Onasch, T. B.,
866 Alfarra, M. R., Prevot, A. S. H., Dommen, J., Duplissy, J., Metzger, A.,
867 Baltensperger, U., and Jimenez, J. L.: O/C and OM/OC ratios of primary,
868 secondary, and ambient organic aerosols with high-resolution time-of-flight
869 aerosol mass spectrometry, *Environ. Sci. Technol.*, 42, 4478-4485,
870 doi:10.1021/es703009q, 2008.

871 Alfarra, M. R., Prevot, A. S. H., Szidat, S., Sandradewi, J., Weimer, S., Lanz, V. A.,
872 Schreiber, D., Mohr, M., and Baltensperger, U.: Identification of the Mass
873 Spectral Signature of Organic Aerosols from Wood Burning Emissions, *Environ.*
874 *Sci. Technol.*, 41, 5770-5777, doi:10.1021/es062289b, 2007.

875 Beekmann, M., Prévôt, A. S. H., Drewnick, F., Sciare, J., Pandis, S. N., Denier van der
876 Gon, H. A. C., Crippa, M., Freutel, F., Poulain, L., Gherzi, V., Rodriguez, E.,
877 Beirle, S., Zotter, P., von der Weiden-Reinmüller, S.-L., Bressi, M., Fountoukis,
878 C., Petetin, H., Szidat, S., Schneider, J., Rosso, A., El Haddad, I., Megaritis, A.,
879 Zhang, Q. J., Michoud, V., Slowik, J. G., Moukhtar, S., Kolmonen, P., Stohl, A.,
880 Eckhardt, S., Borbon, A., Gros, V., Marchand, N., Jaffrezo, J. L.,
881 Schwarzenboeck, A., Colomb, A., Wiedensohler, A., Borrmann, S., Lawrence,
882 M., Baklanov, A., and Baltensperger, U.: In situ, satellite measurement and model
883 evidence on the dominant regional contribution to fine particulate matter levels in
884 the Paris megacity, *Atmos. Chem. Phys.*, 15, 9577-9591, doi:10.5194/acp-15-
885 9577-2015, 2015.

886 Bi, J., Huang, J., Hu, Z., Holben, B. N., and Guo, Z.: Investigating the aerosol optical and
887 radiative characteristics of heavy haze episodes in Beijing during January of 2013,
888 *J. Geophys. Res.*, 119, 9884-9900, doi:10.1002/2014JD021757, 2014.

889 Bond, T., and Bergstrom, R.: Light absorption by carbonaceous particles: An
890 investigative review, *Aerosol. Sci. Tech.*, 40, 27-67,
891 doi:10.1080/02786820500421521, 2006.

- 892 Canagaratna, M. R., Jayne, J. T., Jimenez, J. L., Allan, J. D., Alfarra, M. R., Zhang, Q.,
893 Onasch, T. B., Drewnick, F., Coe, H., Middlebrook, A., Delia, A., Williams, L.
894 R., Trimborn, A. M., Northway, M. J., DeCarlo, P. F., Kolb, C. E., Davidovits, P.,
895 and Worsnop, D. R.: Chemical and microphysical characterization of ambient
896 aerosols with the aerodyne aerosol mass spectrometer, *Mass Spectrom. Rev.*, 26,
897 185-222, doi:10.1002/mas.20115, 2007.
- 898 Canagaratna, M. R., Jimenez, J. L., Kroll, J. H., Chen, Q., Kessler, S. H., Massoli, P.,
899 Hildebrandt Ruiz, L., Fortner, E., Williams, L. R., Wilson, K. R., Surratt, J. D.,
900 Donahue, N. M., Jayne, J. T., and Worsnop, D. R.: Elemental ratio measurements
901 of organic compounds using aerosol mass spectrometry: Characterization,
902 improved calibration, and implications, *Atmos. Chem. Phys.*, 15, 253-272,
903 doi:10.5194/acp-15-253-2015, 2015.
- 904 Canonaco, F., Crippa, M., Slowik, J. G., Baltensperger, U., and Prévôt, A. S. H.: SoFi, an
905 IGOR-based interface for the efficient use of the generalized multilinear engine
906 (ME-2) for the source apportionment: ME-2 application to aerosol mass
907 spectrometer data, *Atmos. Meas. Tech.*, 6, 3649-3661, doi:10.5194/amt-6-3649-
908 2013, 2013.
- 909 Cao, C., Jiang, W., Wang, B., Fang, J., Lang, J., Tian, G., Jiang, J., and Zhu, T. F.:
910 Inhalable Microorganisms in Beijing's PM_{2.5} and PM₁₀ Pollutants during a
911 Severe Smog Event, *Environ. Sci. Technol.*, 48, 1499-1507,
912 doi:10.1021/es4048472, 2014.
- 913 Chan, C. K., and Yao, X.: Air pollution in mega cities in China, *Atmos. Environ.*, 42, 1-
914 42, doi:10.1016/j.atmosenv.2007.09.003, 2008.
- 915 Chen, Y., Zhao, C., Zhang, Q., Deng, Z., Huang, M., and Ma, X.: Aircraft study of
916 Mountain Chimney Effect of Beijing, China, *J. Geophys. Res.*, 114, D08306,
917 10.1029/2008JD010610, 2009.
- 918 Crippa, M., Canonaco, F., Lanz, V. A., Äijälä M., Allan, J. D., Carbone, S., Capes, G.,
919 Ceburnis, D., Dall'Osto, M., Day, D. A., DeCarlo, P. F., Ehn, M., Eriksson, A.,
920 Freney, E., Hildebrandt Ruiz, L., Hillamo, R., Jimenez, J. L., Junninen, H.,
921 Kiendler-Scharr, A., Kortelainen, A. M., Kulmala, M., Laaksonen, A., Mensah,
922 A. A., Mohr, C., Nemitz, E., O'Dowd, C., Ovadnevaite, J., Pandis, S. N., Petäjä
923 T., Poulain, L., Saarikoski, S., Sellegri, K., Swietlicki, E., Tiitta, P., Worsnop, D.
924 R., Baltensperger, U., and Prévôt, A. S. H.: Organic aerosol components derived
925 from 25 AMS data sets across Europe using a consistent ME-2 based source
926 apportionment approach, *Atmos. Chem. Phys.*, 14, 6159-6176, doi:10.5194/acp-
927 14-6159-2014, 2014.
- 928 Crippa, M., DeCarlo, P. F., Slowik, J. G., Mohr, C., Heringa, M. F., Chirico, R., Poulain,
929 L., Freutel, F., Sciare, J., Cozic, J., Di Marco, C. F., Elsasser, M., Nicolas, J. B.,
930 Marchand, N., Abidi, E., Wiedensohler, A., Drewnick, F., Schneider, J.,
931 Borrmann, S., Nemitz, E., Zimmermann, R., Jaffrezo, J. L., Prévôt, A. S. H., and
932 Baltensperger, U.: Wintertime aerosol chemical composition and source

- 933 apporportionment of the organic fraction in the metropolitan area of paris, *Atmos.*
934 *Chem. Phys.*, 13, 961-981, doi:10.5194/acp-13-961-2013, 2013.
- 935 Dall'Osto, M., Ovadnevaite, J., Ceburnis, D., Martin, D., Healy, R. M., O'Connor, I. P.,
936 Kourtchev, I., Sodeau, J. R., Wenger, J. C., and O'Dowd, C.: Characterization of
937 urban aerosol in Cork city (Ireland) using aerosol mass spectrometry, *Atmos.*
938 *Chem. Phys.*, 13, 4997-5015, doi:10.5194/acp-13-4997-2013, 2013.
- 939 DeCarlo, P. F., Kimmel, J. R., Trimborn, A., Northway, M. J., Jayne, J. T., Aiken, A. C.,
940 Gonin, M., Fuhrer, K., Horvath, T., Docherty, K. S., Worsnop, D. R., and
941 Jimenez, J. L.: Field-Deployable, High-Resolution, Time-of-Flight Aerosol Mass
942 Spectrometer, *Anal. Chem.*, 78, 8281-8289, doi:10.1021/ac061249n, 2006.
- 943 Du, W., Sun, Y. L., Xu, Y. S., Jiang, Q., Wang, Q. Q., Yang, W., Wang, F., Bai, Z. P.,
944 Zhao, X. D., and Yang, Y. C.: Chemical characterization of submicron aerosol
945 and particle growth events at a national background site (3295 m a.s.l.) on the
946 Tibetan Plateau, *Atmos. Chem. Phys.*, 15, 10811-10824, doi:10.5194/acp-15-
947 10811-2015, 2015.
- 948 Elser, M., Huang, R. J., Wolf, R., Slowik, J. G., Wang, Q., Canonaco, F., Li, G., Bozzetti,
949 C., Daellenbach, K. R., Huang, Y., Zhang, R., Li, Z., Cao, J., Baltensperger, U.,
950 El-Haddad, I., and Prévôt, A. S. H.: New insights into pm2.5 chemical
951 composition and sources in two major cities in china during extreme haze events
952 using aerosol mass spectrometry, *Atmos. Chem. Phys.*, 16, 3207-3225,
953 doi:10.5194/acp-16-3207-2016, 2016.
- 954 Ge, X., Setyan, A., Sun, Y., and Zhang, Q.: Primary and secondary organic aerosols in
955 Fresno, California during wintertime: Results from high resolution aerosol mass
956 spectrometry, *J. Geophys. Res.*, 117, D19301, doi:10.1029/2012jd018026, 2012.
- 957 Hayes, P. L., Ortega, A. M., Cubison, M. J., Froyd, K. D., Zhao, Y., Cliff, S. S., Hu, W.
958 W., Toohey, D. W., Flynn, J. H., Lefer, B. L., Grossberg, N., Alvarez, S.,
959 Rappenglück, B., Taylor, J. W., Allan, J. D., Holloway, J. S., Gilman, J. B.,
960 Kuster, W. C., de Gouw, J. A., Massoli, P., Zhang, X., Liu, J., Weber, R. J.,
961 Corrigan, A. L., Russell, L. M., Isaacman, G., Worton, D. R., Kreisberg, N. M.,
962 Goldstein, A. H., Thalman, R., Waxman, E. M., Volkamer, R., Lin, Y. H., Surratt,
963 J. D., Kleindienst, T. E., Offenberg, J. H., Dusanter, S., Griffith, S., Stevens, P. S.,
964 Brioude, J., Angevine, W. M., and Jimenez, J. L.: Organic aerosol composition
965 and sources in Pasadena, California during the 2010 CalNex campaign, *J.*
966 *Geophys. Res.*, 118, 9233-9257, doi:10.1002/jgrd.50530, 2013.
- 967 He, K., Yang, F., Ma, Y., Zhang, Q., Yao, X., Chan, C. K., Cadle, S., Chan, T., and
968 Mulawa, P.: The characteristics of PM2.5 in Beijing, China, *Atmos. Environ.*, 35,
969 4959-4970, doi:10.1016/s1352-2310(01)00301-6, 2001.
- 970 He, L.-Y., Huang, X.-F., Xue, L., Hu, M., Lin, Y., Zheng, J., Zhang, R., and Zhang, Y.-
971 H.: Submicron aerosol analysis and organic source apportionment in an urban
972 atmosphere in Pearl River Delta of China using high-resolution aerosol mass
973 spectrometry, *J. Geophys. Res.*, 116, D12304, doi:10.1029/2010jd014566, 2011.

- 974 He, L. Y., Lin, Y., Huang, X. F., Guo, S., Xue, L., Su, Q., Hu, M., Luan, S. J., and Zhang,
975 Y. H.: Characterization of high-resolution aerosol mass spectra of primary organic
976 aerosol emissions from Chinese cooking and biomass burning, *Atmos. Chem.*
977 *Phys.*, 10, 11535-11543, doi:10.5194/acp-10-11535-2010, 2010.
- 978 Herndon, S. C., Onasch, T. B., Wood, E. C., Kroll, J. H., Canagaratna, M. R., Jayne, J.
979 T., Zavala, M. A., Knighton, W. B., Mazzoleni, C., Dubey, M. K., Ulbrich, I. M.,
980 Jimenez, J. L., Seila, R., de Gouw, J. A., de Foy, B., Fast, J., Molina, L. T., Kolb,
981 C. E., and Worsnop, D. R.: Correlation of secondary organic aerosol with odd
982 oxygen in Mexico City, *Geophys. Res. Lett.*, 35, L15804,
983 doi:10.1029/2008GL034058, 2008.
- 984 Hu, W. W., Hu, M., Yuan, B., Jimenez, J. L., Tang, Q., Peng, J. F., Hu, W., Shao, M.,
985 Wang, M., Zeng, L. M., Wu, Y. S., Gong, Z. H., Huang, X. F., and He, L. Y.:
986 Insights on organic aerosol aging and the influence of coal combustion at a
987 regional receptor site of central eastern China, *Atmos. Chem. Phys.*, 13, 10095-
988 10112, doi:10.5194/acp-13-10095-2013, 2013.
- 989 Huang, R.-J., Zhang, Y., Bozzetti, C., Ho, K.-F., Cao, J.-J., Han, Y., Daellenbach, K. R.,
990 Slowik, J. G., Platt, S. M., Canonaco, F., Zotter, P., Wolf, R., Pieber, S. M.,
991 Bruns, E. A., Crippa, M., Ciarelli, G., Piazzalunga, A., Schwikowski, M.,
992 Abbaszade, G., Schnelle-Kreis, J., Zimmermann, R., An, Z., Szidat, S.,
993 Baltensperger, U., Haddad, I. E., and Prevot, A. S. H.: High secondary aerosol
994 contribution to particulate pollution during haze events in China, *Nature*, 514,
995 218-222, doi:10.1038/nature13774, 2014
- 996 Huang, X.-F., Xue, L., Tian, X.-D., Shao, W.-W., Sun, T.-L., Gong, Z.-H., Ju, W.-W.,
997 Jiang, B., Hu, M., and He, L.-Y.: Highly time-resolved carbonaceous aerosol
998 characterization in Yangtze River Delta of China: Composition, mixing state and
999 secondary formation, *Atmos. Environ.*, 64, 200-207,
1000 doi:10.1016/j.atmosenv.2012.09.059, 2013.
- 1001 Huang, X. F., He, L. Y., Hu, M., Canagaratna, M. R., Kroll, J. H., Ng, N. L., Zhang, Y.
1002 H., Lin, Y., Xue, L., Sun, T. L., Liu, X. G., Shao, M., Jayne, J. T., and Worsnop,
1003 D. R.: Characterization of submicron aerosols at a rural site in Pearl River Delta
1004 of China using an Aerodyne High-Resolution Aerosol Mass Spectrometer, *Atmos.*
1005 *Chem. Phys.*, 11, 1865-1877, doi:10.5194/acp-11-1865-2011, 2011.
- 1006 Ianniello, A., Spataro, F., Esposito, G., Allegrini, I., Hu, M., and Zhu, T.: Chemical
1007 characteristics of inorganic ammonium salts in PM_{2.5} in the atmosphere of
1008 Beijing (China), *Atmos. Chem. Phys.*, 11, 10803-10822, doi:10.5194/acp-11-
1009 10803-2011, 2011.
- 1010 Jayne, J. T., Leard, D. C., Zhang, X., Davidovits, P., Smith, K. A., Kolb, C. E., and
1011 Worsnop, D. R.: Development of an Aerosol Mass Spectrometer for Size and
1012 Composition Analysis of Submicron Particles, *Aerosol. Sci. Tech.*, 33, 49 - 70,
1013 doi:10.1080/027868200410840, 2000.
- 1014 Jimenez, J. L., Canagaratna, M. R., Donahue, N. M., Prevot, A. S. H., Zhang, Q., Kroll, J.
1015 H., DeCarlo, P. F., Allan, J. D., Coe, H., Ng, N. L., Aiken, A. C., Docherty, K. S.,

1016 Ulbrich, I. M., Grieshop, A. P., Robinson, A. L., Duplissy, J., Smith, J. D.,
 1017 Wilson, K. R., Lanz, V. A., Hueglin, C., Sun, Y. L., Tian, J., Laaksonen, A.,
 1018 Raatikainen, T., Rautiainen, J., Vaattovaara, P., Ehn, M., Kulmala, M.,
 1019 Tomlinson, J. M., Collins, D. R., Cubison, M. J., E., Dunlea, J., Huffman, J. A.,
 1020 Onasch, T. B., Alfarra, M. R., Williams, P. I., Bower, K., Kondo, Y., Schneider,
 1021 J., Drewnick, F., Borrmann, S., Weimer, S., Demerjian, K., Salcedo, D., Cottrell,
 1022 L., Griffin, R., Takami, A., Miyoshi, T., Hatakeyama, S., Shimono, A., Sun, J. Y.,
 1023 Zhang, Y. M., Dzepina, K., Kimmel, J. R., Sueper, D., Jayne, J. T., Herndon, S.
 1024 C., Trimborn, A. M., Williams, L. R., Wood, E. C., Middlebrook, A. M., Kolb, C.
 1025 E., Baltensperger, U., and Worsnop, D. R.: Evolution of organic aerosols in the
 1026 atmosphere, *Science*, 326, 1525-1529, doi:10.1126/science.1180353, 2009.

1027 Liu, Z., Wang, Y., Vrekoussis, M., Richter, A., Wittrock, F., Burrows, J. P., Shao, M.,
 1028 Chang, C.-C., Liu, S.-C., Wang, H., and Chen, C.: Exploring the missing source
 1029 of glyoxal (CHOCHO) over China, *Geophys. Res. Lett.*, 39, L10812,
 1030 doi:10.1029/2012GL051645, 2012.

1031 Minguillón, M. C., Perron, N., Querol, X., Szidat, S., Fahrni, S. M., Alastuey, A.,
 1032 Jimenez, J. L., Mohr, C., Ortega, A. M., Day, D. A., Lanz, V. A., Wacker, L.,
 1033 Reche, C., Cusack, M., Amato, F., Kiss, G., Hoffer, A., Decesari, S., Moretti, F.,
 1034 Hillamo, R., Teinilä K., Seco, R., Peñuelas, J., Metzger, A., Schallhart, S.,
 1035 Müller, M., Hansel, A., Burkhardt, J. F., Baltensperger, U., and Prévôt, A. S. H.:
 1036 Fossil versus contemporary sources of fine elemental and organic carbonaceous
 1037 particulate matter during the DAURE campaign in Northeast Spain, *Atmos.*
 1038 *Chem. Phys.*, 11, 12067-12084, doi:10.5194/acp-11-12067-2011, 2011.

1039 Mohr, C., DeCarlo, P. F., Heringa, M. F., Chirico, R., Slowik, J. G., Richter, R., Reche,
 1040 C., Alastuey, A., Querol, X., Seco, R., Penuelas, J., Jimenez, J. L., Crippa, M.,
 1041 Zimmermann, R., Baltensperger, U., and Prevot, A. S. H.: Identification and
 1042 quantification of organic aerosol from cooking and other sources in Barcelona
 1043 using aerosol mass spectrometer data, *Atmos. Chem. Phys.*, 12, 1649-1665,
 1044 doi:10.5194/acp-12-1649-2012, 2012.

1045 Ng, N. L., Canagaratna, M. R., Zhang, Q., Jimenez, J. L., Tian, J., Ulbrich, I. M., Kroll, J.
 1046 H., Docherty, K. S., Chhabra, P. S., Bahreini, R., Murphy, S. M., Seinfeld, J. H.,
 1047 Hildebrandt, L., Donahue, N. M., DeCarlo, P. F., Lanz, V. A., Prévôt, A. S. H.,
 1048 Dinar, E., Rudich, Y., and Worsnop, D. R.: Organic aerosol components observed
 1049 in Northern Hemispheric datasets from Aerosol Mass Spectrometry, *Atmos.*
 1050 *Chem. Phys.*, 10, 4625-4641, doi:10.5194/acp-10-4625-2010, 2010.

1051 Ortega, A. M., Day, D. A., Cubison, M. J., Brune, W. H., Bon, D., de Gouw, J. A., and
 1052 Jimenez, J. L., Secondary organic aerosol formation and primary organic aerosol
 1053 oxidation from biomass-burning smoke in a flow reactor during FLAME-3,
 1054 *Atmos. Chem. Phys.*, 13(22), 11551-11571, doi:10.5194/acp-13-11551-2013,
 1055 2013.

1056 Paatero, P., and Tapper, U.: Positive matrix factorization: A non-negative factor model
 1057 with optimal utilization of error estimates of data values, *Environmetrics*, 5,
 1058 doi:111-126, 10.1002/env.3170050203, 1994.

- 1059 Song, Y., Xie, S., Zhang, Y., Zeng, L., Salmon, L. G., and Zheng, M.: Source
1060 apportionment of PM_{2.5} in Beijing using principal component analysis/absolute
1061 principal component scores and UNMIX, *Sci. Total. Environ.*, 372, 278-286,
1062 doi:10.1016/j.scitotenv.2006.08.041, 2006.
- 1063 Sun, Y., Du, W., Fu, P., Wang, Q., Li, J., Ge, X., Zhang, Q., Zhu, C., Ren, L., Xu, W.,
1064 Zhao, J., Han, T., Worsnop, D. R., and Wang, Z.: Primary and secondary aerosols
1065 in Beijing in winter: sources, variations and processes, *Atmos. Chem. Phys.*
1066 *Discuss.*, 1-41, 10.5194/acp-2016-255, 2016.
- 1067 Sun, Y., Jiang, Q., Wang, Z., Fu, P., Li, J., Yang, T., and Yin, Y.: Investigation of the
1068 sources and evolution processes of severe haze pollution in Beijing in January
1069 2013, *J. Geophys. Res.*, 119, 2014JD021641, doi:10.1002/2014JD021641, 2014.
- 1070 Sun, Y., Zhuang, G., Tang, A., Wang, Y., and An, Z.: Chemical Characteristics of PM_{2.5}
1071 and PM₁₀ in Haze-Fog Episodes in Beijing, *Environ. Sci. Technol.*, 40, 3148-
1072 3155, doi:10.1021/es051533g, 2006.
- 1073 Sun, Y., Zhang, Q., Zheng, M., Ding, X., Edgerton, E. S., and Wang, X.: Characterization
1074 and source apportionment of water-soluble organic matter in atmospheric fine
1075 particles (pm_{2.5}) with high-resolution aerosol mass spectrometry and gc-ms,
1076 *Environ. Sci. and Technol.*, 45, 4854 - 4861, doi:10.1021/es200162h, 2011a.
- 1077 Sun, Y., Zhang, Q., Schwab, J. J., Demerjian, K. L., Chen, W. N., Bae, M. S., Hung, H.
1078 M., Hogrefe, O., Frank, B., Rattigan, O. V., and Lin, Y. C.: Characterization of
1079 the sources and processes of organic and inorganic aerosols in New York city
1080 with a high-resolution time-of-flight aerosol mass spectrometer, *Atmos. Chem.*
1081 *Phys.*, 11, 1581-1602, doi:10.5194/acp-11-1581-2011, 2011b.
- 1082 Sun, Y. L., Wang, Z., Fu, P., Jiang, Q., Yang, T., Li, J., and Ge, X.: The impact of
1083 relative humidity on aerosol composition and evolution processes during
1084 wintertime in Beijing, China, *Atmos. Environ.*, 77, 927-934,
1085 doi:10.1016/j.atmosenv.2013.06.019, 2013a.
- 1086 Sun, Y. L., Wang, Z. F., Fu, P. Q., Yang, T., Jiang, Q., Dong, H. B., Li, J., and Jia, J. J.:
1087 Aerosol composition, sources and processes during wintertime in Beijing, China,
1088 *Atmos. Chem. Phys.*, 13, 4577-4592, doi:10.5194/acp-13-4577-2013, 2013b.
- 1089 Szidat, S.; Salazar, G. A.; Vogel, E.; Battaglia, M.; Wacker, L.; Synal, H. A.; Türlér, A.:
1090 ¹⁴C analysis and sample preparation at the new Bern Laboratory for the Analysis
1091 of Radiocarbon with AMS (LARA). *Radiocarbon*, 56, 561-566,
1092 doi:10.2458/56.17457, 2014.
- 1093 Tang, X. Y., Tian, B. S., Chen, C. H., and Ren, Z. H.: A study of photochemical smog
1094 pollution and its control stratiges at Xi-Gu district of Lanzhou city, China
1095 *Environ. Sci.*, 5(2), 1-11, 1985. (in Chinese with abstract in English)
- 1096 Ulbrich, I. M., Canagaratna, M. R., Zhang, Q., Worsnop, D. R., and Jimenez, J. L.:
1097 Interpretation of organic components from Positive Matrix Factorization of
1098 aerosol mass spectrometric data, *Atmos. Chem. Phys.*, 9, 2891-2918,
1099 doi:10.5194/acp-9-2891-2009, 2009.

- 1100 Volkamer, R., Jimenez, J. L., San Martini, F., Dzepina, K., Zhang, Q., Salcedo, D.,
1101 Molina, L. T., Worsnop, D. R., and Molina, M. J.: Secondary organic aerosol
1102 formation from anthropogenic air pollution: Rapid and higher than expected,
1103 *Geophys. Res. Lett.*, 33, L17811, doi:10.1029/2006GL026899, 2006.
- 1104 Wang, X., Cotter, E., Iyer, K. N., Fang, J., Williams, B. J., and Biswas, P.: Relationship
1105 between pyrolysis products and organic aerosols formed during coal combustion,
1106 *P. Combust. Inst.*, 35, 2347-2354, doi:10.1016/j.proci.2014.07.073, 2015.
- 1107 Wang, Y., Ying, Q., Hu, J., and Zhang, H.: Spatial and temporal variations of six criteria
1108 air pollutants in 31 provincial capital cities in China during 2013–2014, *Environ.*
1109 *Int.*, 73, 413-422, doi:10.1016/j.envint.2014.08.016, 2014.
- 1110 Wiedensohler, A., Birmili, W., Nowak, A., Sonntag, A., Weinhold, K., Merkel, M.,
1111 Wehner, B., Tuch, T., Pfeifer, S., Fiebig, M., Fj äraa, A. M., Asmi, E., Sellegri, K.,
1112 Depuy, R., Venzac, H., Villani, P., Laj, P., Aalto, P., Ogren, J. A., Swietlicki, E.,
1113 Williams, P., Roldin, P., Quincey, P., Hüglin, C., Fierz-Schmidhauser, R., Gysel,
1114 M., Weingartner, E., Riccobono, F., Santos, S., Grüning, C., Faloon, K.,
1115 Beddows, D., Harrison, R., Monahan, C., Jennings, S. G., O'Dowd, C. D.,
1116 Marinoni, A., Horn, H. G., Keck, L., Jiang, J., Scheckman, J., McMurry, P. H.,
1117 Deng, Z., Zhao, C. S., Moerman, M., Henzing, B., de Leeuw, G., Lösschau, G.,
1118 and Bastian, S.: Mobility particle size spectrometers: harmonization of technical
1119 standards and data structure to facilitate high quality long-term observations of
1120 atmospheric particle number size distributions, *Atmos. Meas. Tech.*, 5, 657-685,
1121 doi:10.5194/amt-5-657-2012, 2012.
- 1122 Wood, E. C., Canagaratna, M. R., Herndon, S. C., Onasch, T. B., Kolb, C. E., Worsnop,
1123 D. R., Kroll, J. H., Knighton, W. B., Seila, R., Zavala, M., Molina, L. T.,
1124 DeCarlo, P. F., Jimenez, J. L., Weinheimer, A. J., Knapp, D. J., Jobson, B. T.,
1125 Stutz, J., Kuster, W. C., and Williams, E. J.: Investigation of the correlation
1126 between odd oxygen and secondary organic aerosol in Mexico City and Houston,
1127 *Atmos. Chem. Phys.*, 10, 8947-8968, doi:10.5194/acp-10-8947-2010, 2010.
- 1128 Xu, J., Zhang, Q., Chen, M., Ge, X., Ren, J., and Qin, D.: Chemical composition, sources,
1129 and processes of urban aerosols during summertime in northwest China: insights
1130 from high-resolution aerosol mass spectrometry, *Atmos. Chem. Phys.*, 14, 12593-
1131 12611, doi:10.5194/acp-14-12593-2014, 2014.
- 1132 Young, D., Kim, H. J., Parworth, C., Zhou, S., Zhang, X. L., Cappa, C., Seco, R., Kim,
1133 S., and Zhang, Q.: Influences of emission sources and meteorology on aerosol
1134 chemistry in a polluted urban environment: Results from discover-aq california,
1135 *Atmospheric Chemistry & Physics Discussions*, 15, 35057-35115,
1136 doi:10.5194/acpd-15-35057-2015, 2015.
- 1137 Yu, L., Wang, G., Zhang, R., Zhang, L., Song, Y., Wu, B., Li, X., An, K., and Chu, J.:
1138 Characterization and Source Apportionment of PM_{2.5} in an Urban Environment
1139 in Beijing, *Aerosol Air Qual. Res.*, 13, 574-583, doi:10.4209/aaqr.2012.07.0192,
1140 2013.

- 1141 Zhang, J. K., Sun, Y., Liu, Z. R., Ji, D. S., Hu, B., Liu, Q., and Wang, Y. S.:
1142 Characterization of submicron aerosols during a month of serious pollution in
1143 Beijing, 2013, *Atmos. Chem. Phys.*, 14, 2887-2903, doi:10.5194/acp-14-2887-
1144 2014, 2014.
- 1145 Zhang, L., Chen, C., Li, S., and Zhang, F.: Air pollution and potential control schemes in
1146 Lanzhou, *Res. Environ. Sci.*, 13(4), 18-21, 2000.
- 1147 Zhang, Q., Canagaratna, M. R., Jayne, J. T., Worsnop, D. R., and Jimenez, J. L.: Time-
1148 and size-resolved chemical composition of submicron particles in Pittsburgh:
1149 Implications for aerosol sources and processes, *J. Geophys. Res.*, 110, D07s09,
1150 doi:10.1029/2004jd004649, 2005.
- 1151 Zhang, Q., Jimenez, J. L., Canagaratna, M. R., Ulbrich, I. M., Ng, N. L., Worsnop, D. R.,
1152 and Sun, Y.: Understanding atmospheric organic aerosols via factor analysis of
1153 aerosol mass spectrometry: a review, *Anal. Bioanal. Chem.*, 401, 3045-3067,
1154 doi:10.1007/s00216-011-5355-y, 2011a.
- 1155 Zhang, Q., and Li, H.: A study of the relationship between air pollutants and inversion in
1156 the ABL over the city of Lanzhou, *Adv. Atmos. Sci.*, 28(4), 879-886, doi:
1157 10.1007/s00376-010-0079-z, 2011b.
- 1158 Zhang, R., Jing, J., Tao, J., Hsu, S. C., Wang, G., Cao, J., Lee, C. S. L., Zhu, L., Chen, Z.,
1159 Zhao, Y., and Shen, Z.: Chemical characterization and source apportionment of
1160 PM_{2.5} in Beijing: seasonal perspective, *Atmos. Chem. Phys.*, 13, 7053-7074,
1161 doi:10.5194/acp-13-7053-2013, 2013.
- 1162 Zhang, Y., Schauer, J. J., Zhang, Y., Zeng, L., Wei, Y., Liu, Y., and Shao, M.:
1163 Characteristics of Particulate Carbon Emissions from Real-World Chinese Coal
1164 Combustion, *Environ. Sci. Technol.*, 42, 5068-5073, doi:10.1021/es7022576,
1165 2008.
- 1166 Zhang, Y. J., Tang, L. L., Wang, Z., Yu, H. X., Sun, Y. L., Liu, D., Qin, W., Canonaco,
1167 F., Prévôt, A. S. H., Zhang, H. L., and Zhou, H. C.: Insights into characteristics,
1168 sources, and evolution of submicron aerosols during harvest seasons in the
1169 Yangtze River delta region, China, *Atmos. Chem. Phys.*, 15, 1331-1349,
1170 doi:10.5194/acp-15-1331-2015, 2015a.
- 1171 Zhang, Y. L., Huang, R. J., El Haddad, I., Ho, K. F., Cao, J. J., Han, Y., Zotter, P.,
1172 Bozzetti, C., Daellenbach, K. R., Canonaco, F., Slowik, J. G., Salazar, G.,
1173 Schwikowski, M., Schnelle-Kreis, J., Abbaszade, G., Zimmermann, R.,
1174 Baltensperger, U., Prévôt, A. S. H., and Szidat, S.: Fossil vs. Non-fossil sources of
1175 fine carbonaceous aerosols in four Chinese cities during the extreme winter haze
1176 episode of 2013, *Atmos. Chem. Phys.*, 15, 1299-1312, 10.5194/acp-15-1299-
1177 2015, 2015b.
- 1178 Zhang, Y. L.; Perron, N.; Ciobanu, V. G.; Zotter, P.; Minguillón, M. C.; Wacker, L.;
1179 Prévôt, A. S. H.; Baltensperger, U.; Szidat, S.: On the isolation of OC and EC and
1180 the optimal strategy of radiocarbon-based source apportionment of carbonaceous

- 1181 aerosols. *Atmos. Chem. Phys.*, 12, 10841-10856, doi:10.5194/acp-12-10841-
1182 2012, 2012.
- 1183 Zhang, Z., Wang, X., Zhang, Y., Lü, S., Huang, Z., Huang, X., and Wang, Y.: Ambient
1184 air benzene at background sites in China's most developed coastal regions:
1185 Exposure levels, source implications and health risks, *Sci. Total. Environ.*, 511,
1186 792-800, doi:10.1016/j.scitotenv.2015.01.003, 2015c.
- 1187 Zhao, X. J., Zhao, P. S., Xu, J., Meng, W., Pu, W. W., Dong, F., He, D., and Shi, Q. F.:
1188 Analysis of a winter regional haze event and its formation mechanism in the
1189 North China Plain, *Atmos. Chem. Phys.*, 13, 5685-5696, doi:10.5194/acp-13-
1190 5685-2013, 2013.
- 1191 Zheng, M., Salmon, L. G., Schauer, J. J., Zeng, L., Kiang, C. S., Zhang, Y., and Cass, G.
1192 R.: Seasonal trends in PM_{2.5} source contributions in Beijing, China, *Atmos.*
1193 *Environ.*, 39, 3967-3976, doi:10.1016/j.atmosenv.2005.03.036, 2005.
- 1194 Zotter, P., El-Haddad, I., Zhang, Y., Hayes, P. L., Zhang, X., Lin, Y.-H., Wacker, L.,
1195 Schnelle-Kreis, J., Abbaszade, G., Zimmermann, R., Surratt, J. D., Weber, R.,
1196 Jimenez, J. L., Szidat, S., Baltensperger, U., and Prévôt, A. S. H.: Diurnal cycle of
1197 fossil and nonfossil carbon using radiocarbon analyses during CalNex, *Journal of*
1198 *Geophysical Research: Atmospheres*, 119, 6818-6835,
1199 doi:10.1002/2013JD021114, 2014.

1200

1201 Table 1 Comparison of the composition of category ions and elemental composition of

1202 OA between winter 2013/2014 and summer 2012.

1203

Category Ions	Winter 2014	Summer 2012
$C_xH_y^+$	61%	56%
$C_xH_yO_1^+$	25%	27%
$C_xH_yO_2^+$	9%	11%
$C_xH_yN_p^+$	3%	3%
$C_xH_yN_pO_z^+$	0	1%
$H_yO_1^+$	2%	2%
Elemental composition		
C	66%	59%
H	8%	7%
O	25%	26%
N	1%	1%

1204

1205 Table 2 Correlation coefficient (r) between time series of OA factors and other aerosol

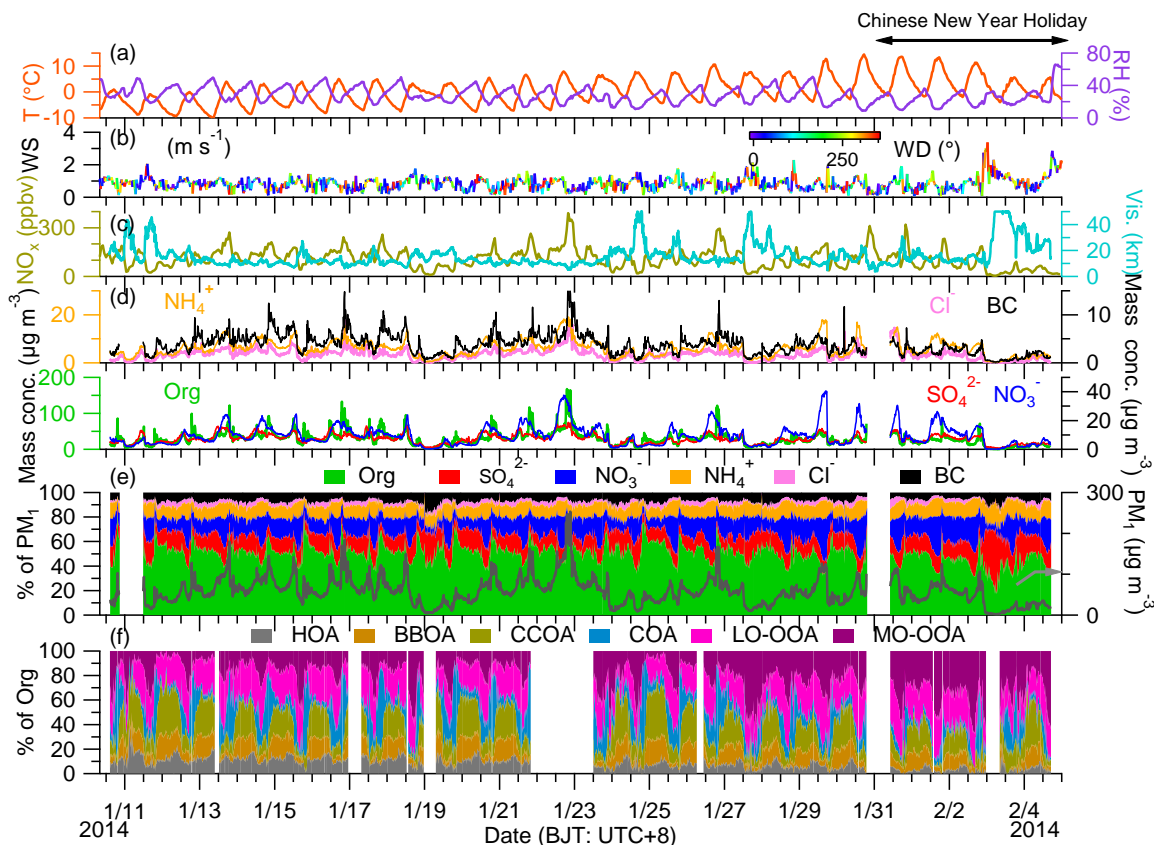
1206 species.

r	HOA	BBOA	COA	CCOA	LO-OOA	MO-OOA	POA*	SOA*
BC	0.84	0.75	0.43	0.74	0.59	0.14	0.75	0.44
PAH	0.69	0.75	0.46	0.73	0.27	-0.07	0.75	0.13
Sulphate	0.69	0.35	0.32	0.32	0.89	0.56	0.49	0.84
Nitrate	0.35	0.06	0.31	0.06	0.77	0.84	0.31	0.90
Chloride	0.75	0.62	0.33	0.62	0.79	0.30	0.61	0.64
Sulphate + Nitrate	0.50	0.17	0.34	0.16	0.86	0.79	0.40	0.93
Sulphate + Nitrate + Chloride	0.59	0.29	0.35	0.29	0.89	0.70	0.47	0.91

1207

* POA = HOA + BBOA + COA + CCOA, SOA = LO-OOA + MO-OOA

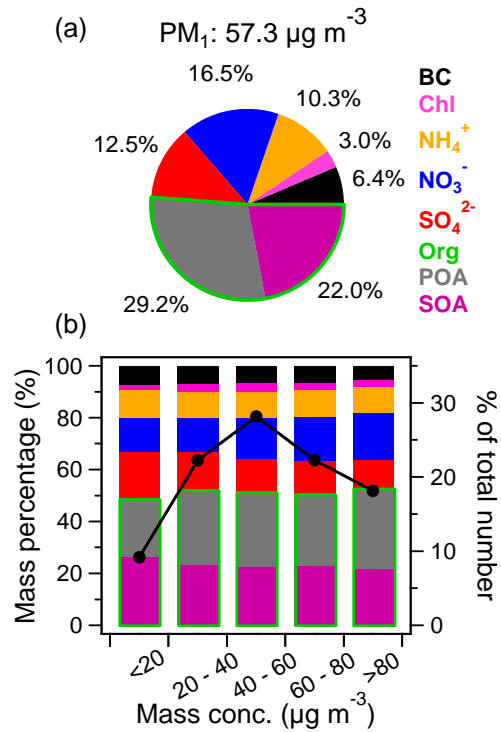
1208



1209
 1210
 1211
 1212
 1213
 1214
 1215
 1216

Fig. 1 Summary of meteorological and aerosol species data. (a) air temperature (T) and relative humidity (RH), (b) wind speed (WS) colored by wind direction (WD), (c) NO_x and visibility, (d) mass concentration of PM₁ species (BC is from aethalometer measurement), and (f) the mass contribution of organic components to organic aerosol. Note that BC is from aethalometer measurement.

1217

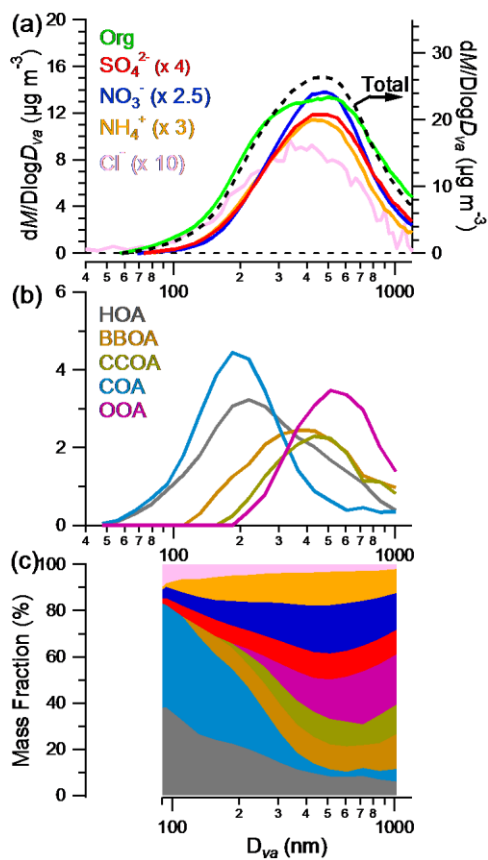


1218

1219

1220 Fig. 2 The average mass contribution of PM_1 (= NR- PM_1 + BC) species (a) during the
1221 whole sampling period and (b) as a function of the PM_1 mass concentration ($\mu g m^{-3}$) bins
1222 (left). The right axis in (b) shows the accumulated data number in each bin. The organics
1223 were decomposed into primary organic aerosol (POA) and secondary organic aerosol
1224 (SOA) using PMF (section 3.4).

1225

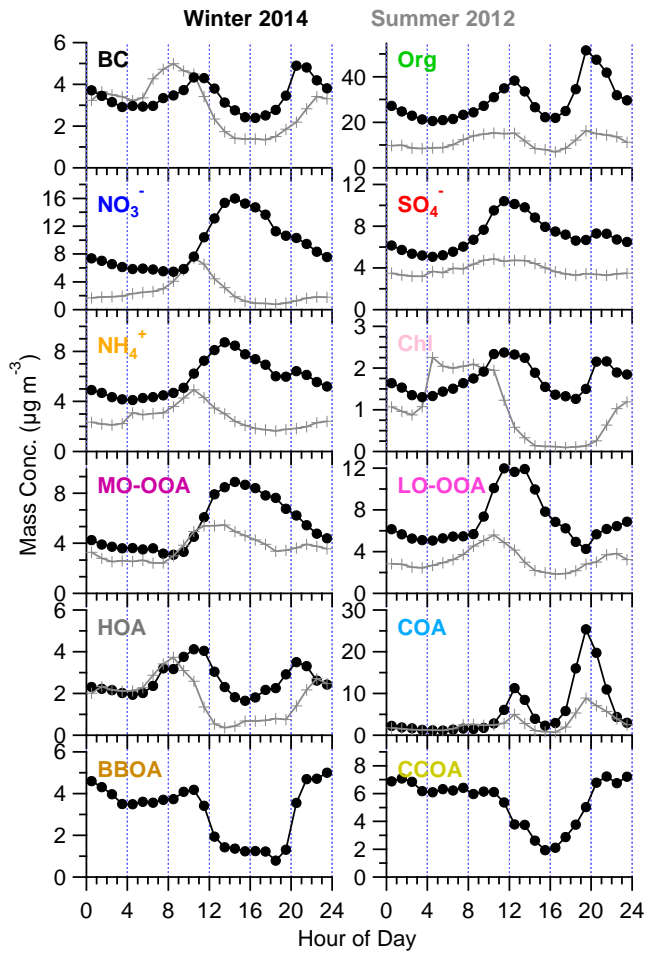


1226

1227 Fig. 3 The size distributions of (a) NR-PM₁ species, (b) organic components, and mass

1228 contribution of all species to NR-PM₁.

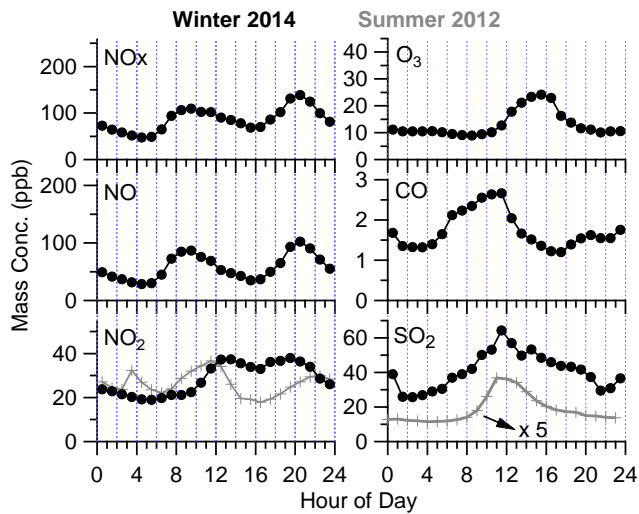
1229



1230

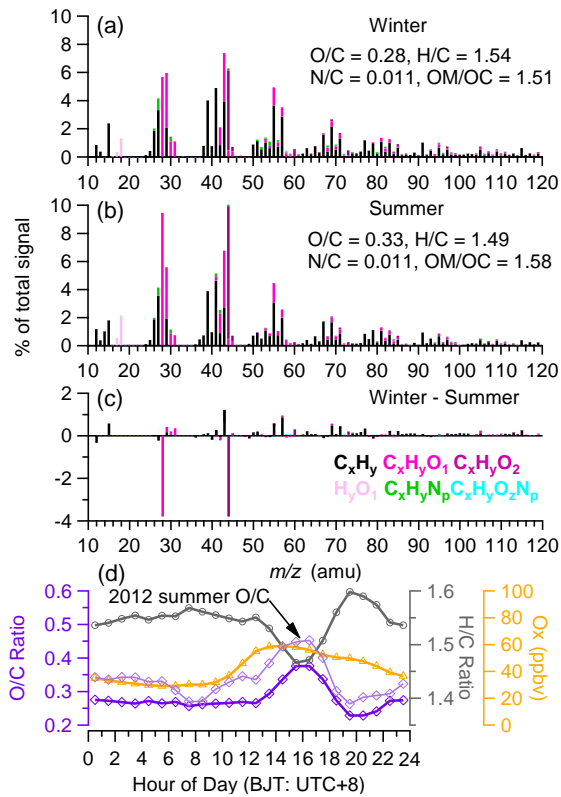
1231 Fig. 4 The diurnal variation of PM₁ species during winter 2013/2014 and summer 2012.

1232

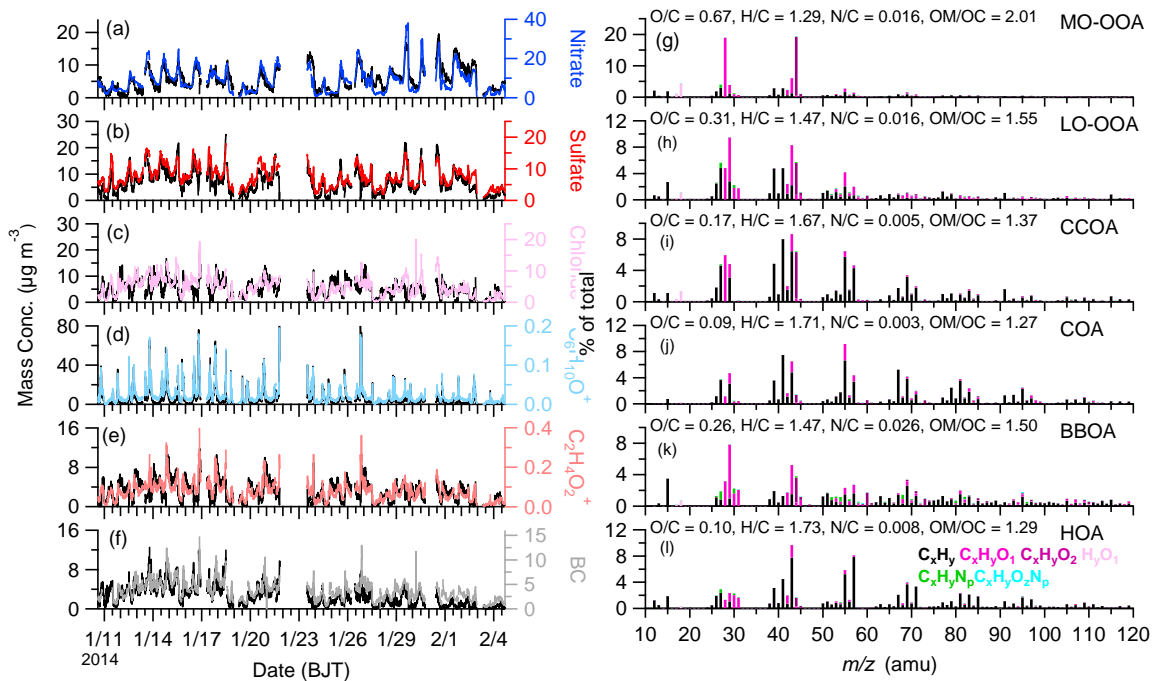


1233

1234 Fig. 5 The diurnal variations of gas species downloaded from MEP-China station during
 1235 winter 2013/2014 and summer 2012.
 1236



1237
 1238 Fig. 6 The average HR-MS and elemental ratios of organics for (a) this study, (b) summer
 1239 2012, (c) the HR-MS difference between this study and summer 2012, and (d) the
 1240 diurnal variations of elemental ratios and odd oxygen ($Ox = NO_2 + O_3$).
 1241

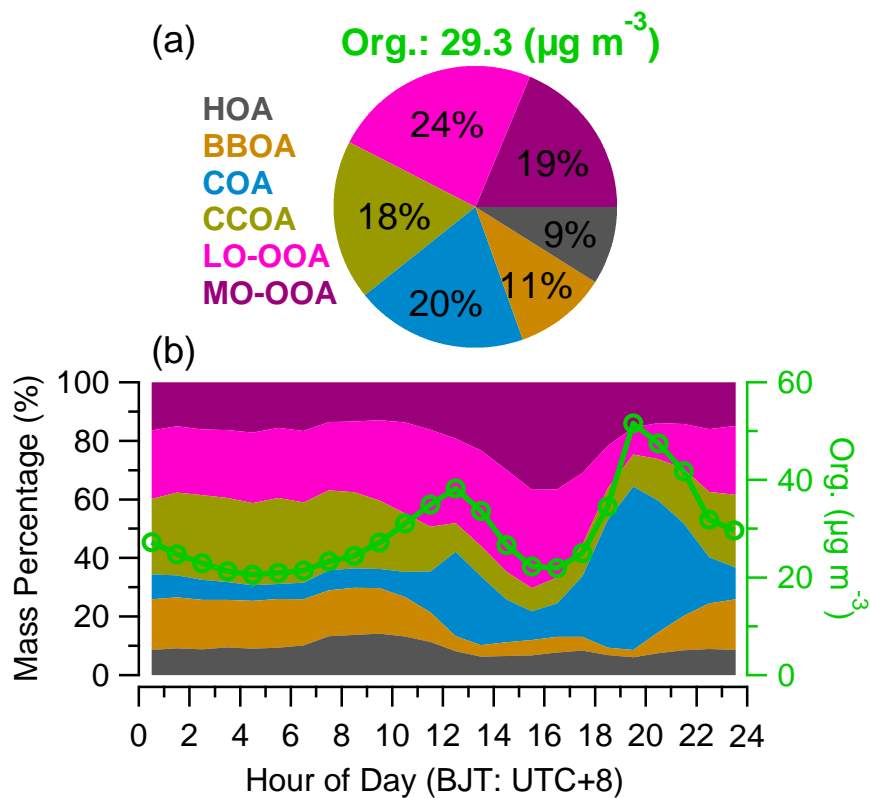


1242

1243 Fig. 7 The PMF results of time series (a – f) and HR-MS (g – l) for each component. The

1244 temporal variations of different tracers are also present for supporting each component.

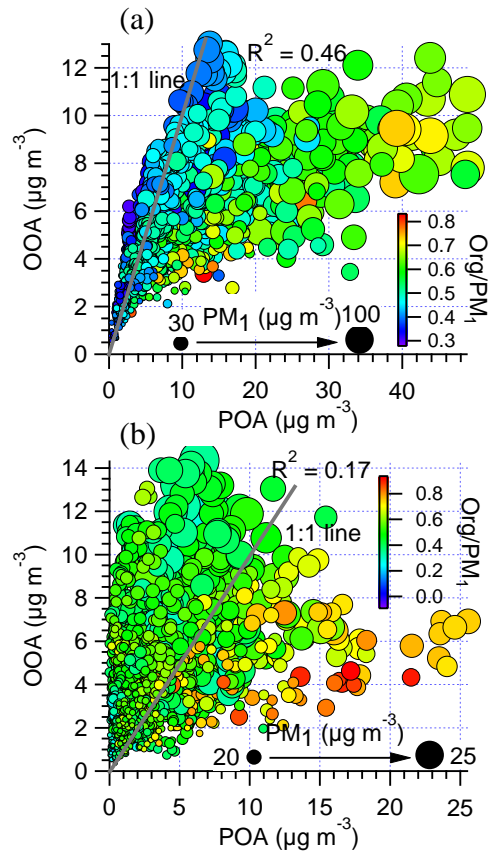
1245



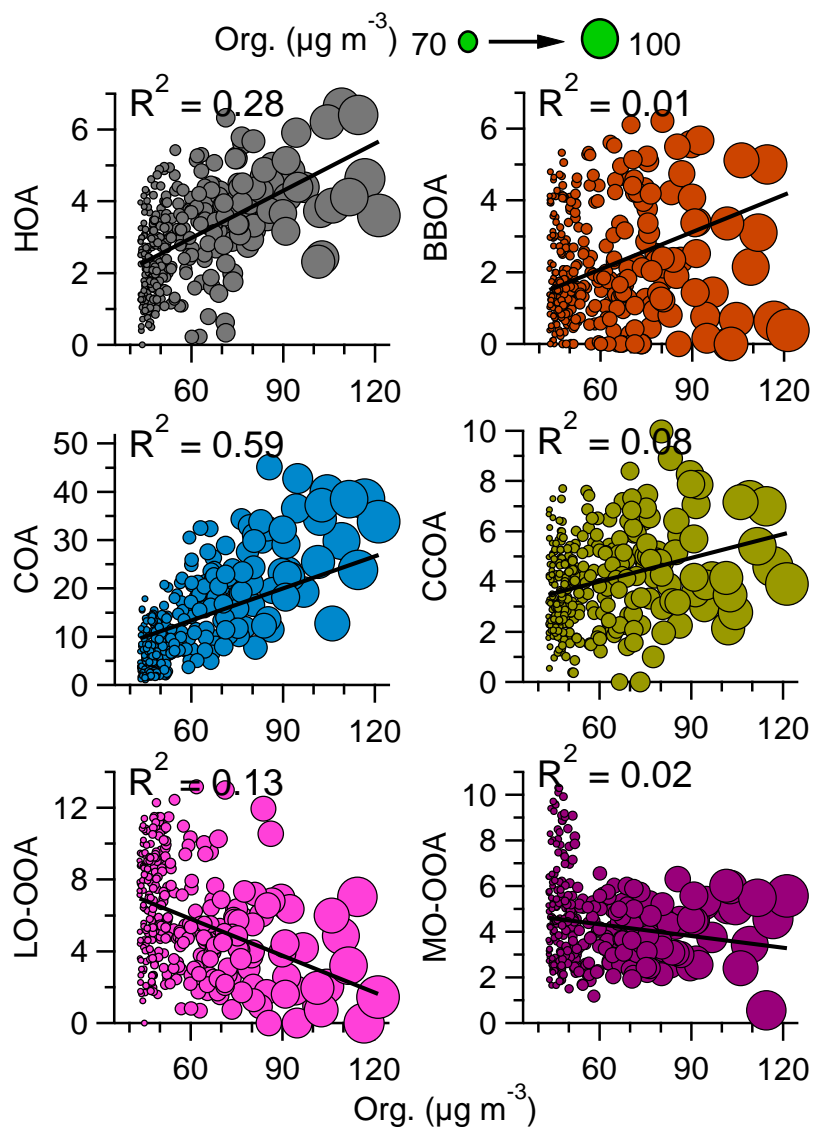
1246

1247 Fig. 8 (a) The average mass concentration of organics and mass contributions of organic
1248 components to organics, and (b) the diurnal variations of organic components and
1249 organics.
1250

1251
1252



1253
1254 Fig. 9 The scatter plot of OOA and POA colored by the ratio of $\text{Org}/\text{PM}_{10}$ and sized by the
1255 mass concentration of PM_{10} for (a) winter 2013/2014 and (b) summer 2012.
1256

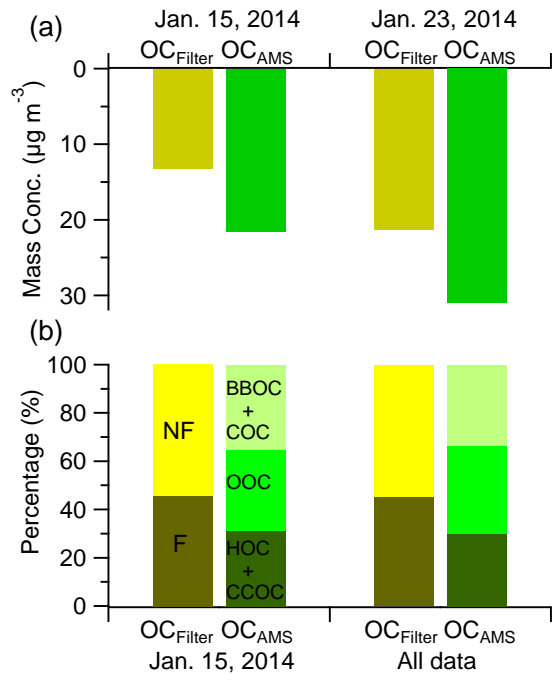


1257

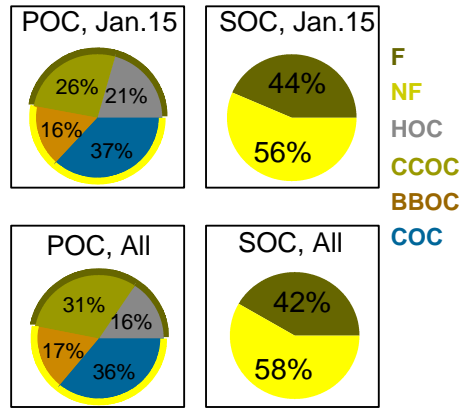
1258 Fig. 10 The scatter plots of each organic component ($\mu\text{g m}^{-3}$) versus organics during haze

1259 periods (definite as organics $> 43 \mu\text{g m}^{-3}$ ($\text{Org_avg} + 1\sigma$))

1260



1261
 1262 Fig. 11 (a) The comparisons of (a) OC concentration measured by filter sample ($\text{OC}_{\text{Filter}}$)
 1263 and AMS (OC_{AMS}) on Jan. 15 and 23, 2014 and (b) the non-fossil (NF) and fossil (F)
 1264 carbon fraction measured by ^{14}C and OC components in AMS.
 1265



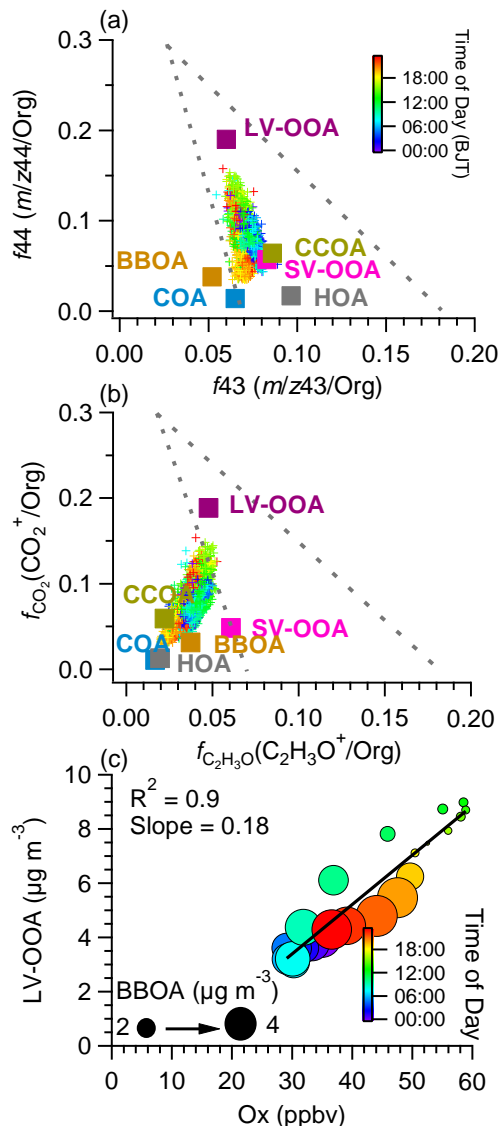
1266

1267

Fig. 12 The non-fossil (NF) and fossil (F) carbon fraction in POC and SOC during Jan. 15 and all data of AMS.

1268

1269



1270

1271 Fig. 13 Triangle plot of f_{44} (fraction of m/z 44 in organics) vs f_{43} (fraction of m/z 43 in

1272 organics) and (b) $f_{\text{CO}_2^+}$ (fraction of CO_2^+ in organics) vs. $f_{\text{C}_2\text{H}_3\text{O}^+}$ (fraction of $\text{C}_2\text{H}_3\text{O}^+$ in

1273 organics) for OA and six OA factors, and (c) scatter plot of MO-OOA vs. O_x (the sum of

1274 O_3 and NO_2) with linear fit and colored by time of day.

1275

1276